Changes in Corticotrope Gene Expression Upon Increased Expression of Peptidylglycine α-Amidating Monooxygenase

Richard E. Mains,[1] Crysten Blaby-Haas,[2] Bruce A. Rheaume,[1] and Betty A. Eipper[1,3]

[1]Neuroscience, University of Connecticut Health Center, Farmington, Connecticut 06030; [2]Biology, Brookhaven National Laboratory, Upton, New York 11973; and [3]Molecular Biology & Biophysics, University of Connecticut, Farmington, Connecticut 06030

Throughout evolution, secretion has played an essential role in the ability of organisms and single cells to survive in the face of a changing environment. Peptidylglycine α-amidating monooxygenase (PAM) is an integral membrane monooxygenase, first identified for its role in the biosynthesis of neuroendocrine peptides released by the regulated secretory pathway. PAM was subsequently identified in *Chlamydomonas reinhardtii*, a unicellular green alga, where it plays an essential role in constitutive secretion and in ciliogenesis. Reduced expression of *C. reinhardtii* PAM resulted in significant changes in secretion and ciliogenesis. Hence, a screen was performed for transcripts and proteins whose expression responded to changes in PAM levels in a mammalian corticotrope tumor cell line. The goal was to identify genes not previously known to play a role in secretion. The screen identified transcription factors, peptidyl prolyl isomerases, endosomal/lysosomal proteins, and proteins involved in tissue-specific responses to glucose and amino acid availability that had not previously been recognized as relevant to the secretory pathway. Perhaps reflecting the dependence of PAM on molecular oxygen, many PAM-responsive genes are known to be hypoxia responsive. The data highlight the extent to which the performance of the secretory pathway may be integrated into a wide diversity of signaling pathways. **(*Endocrinology* 159: 2621–2639, 2018)**

Bacteria, plants, and animals secrete peptides as a means of defense, recognition of self vs nonself and communication (1–4). The production of many of these peptides proceeds through the classical, signal peptide-mediated pathway. The cellular machinery needed for protein folding, disulfide bond formation, glycosylation, and quality control plays an essential role in preparing precursors for transit through the secretory pathway. The production of product peptides frequently requires the participation of multiple proteases. Amidation of the COOH-terminus of a peptide, which is often essential for biological activity, requires the participation of peptidylglycine α-amidating monooxygenase (PAM; EC 1.14.17.3), a copper-, zinc-, and ascorbate-dependent enzyme (5–7). Peptide secretion in multicellular organisms requires cell type–specific integration of a wide variety of inputs. In addition to rapid changes in peptide secretion, physiological stimuli often trigger coordinated changes

ISSN Online 1945-7170

Received 7 March 2018. Accepted 9 May 2018.
First Published Online 16 May 2018

Abbreviations: Actb, β-actin; Atf3, activating transcription factor 3; Atg9b, autophagy-related protein 9b; Chac1, glutathione-specific γ-glutamyl-cyclotransferase 1; Creb1, cAMP-responsive element binding protein 1; CRH, corticotropin-releasing hormone; CSFM, complete serum-free medium; ER, endoplasmic reticulum; FKBP, FK506 binding protein; FPKM, fragments per kilobase of transcript per million mapped reads; Gapdh, glyceraldehyde 3-phosphate dehydrogenase; Hprt, hypoxanthine guanine phosphoribosyl transferase; HSG, HEPES-saline-glucose; HIF, hypoxia-inducible factor; Hsp90, heat shock protein 90; IPA, Ingenuity Pathway Analysis; iPAM, induced peptidylglycine α-amidating monooxygenase; LAMP, lysosomal/endosomal-associated membrane glycoprotein; Ndrg1, *N*-myc downstream regulated gene 1; PAL, peptidyl-α-hydroxyglycine α-amidating lyase; PAM, peptidylglycine α-amidating monooxygenase; PHM, peptidylglycine α-hydroxylating monooxygenase; Ppia, peptidylprolyl isomerase A; POMC, proopiomelanocortin; PPIase, peptidyl prolyl isomerase; qPCR, quantitative PCR; RNA-seq, RNA sequencing; Sdha, succinate dehydrogenase subunit a; sfCD, soluble fragment of the COOH-terminal domain; Tlr3, Toll-like receptor 3; TPR, tetratricopeptide repeat; Txnip, thioredoxin-interacting protein; Wt, wild-type.

in the production of peptide precursors and their processing enzymes. For example, melanotropes increase expression of proopiomelanocortin (POMC), prohormone convertases 1 and 2, and PAM when stimulated (8).

The two enzymatic domains of PAM, peptidylglycine α-hydroxylating monooxygenase (PHM) and peptidyl-α-hydroxyglycine α-amidating lyase (PAL), catalyze the sequential conversion of a peptidylglycine substrate into a peptidyl-α-hydroxylglycine intermediate, followed by cleavage of the *N*-Cα bond in glycine, producing amidated peptide plus glyoxylate. When expressed individually, both catalytic domains of PAM are active, and each is efficiently stored in secretory granules. Although this finding suggests that PHM and PAL activities do not need to be encoded by the same gene, species ranging from human to *Chlamydomonas reinhardtii*, a unicellular green alga, express bifunctional integral membrane PAM proteins (6, 7), leading to the prediction that a similar enzyme was present in the last eukaryotic common ancestor (5, 9). When PAM, a type 1 integral membrane enzyme, reaches the plasma membrane, it undergoes endocytosis, a pathway thought to have been well developed before the divergence of plants and animals (10, 11). In mammalian cells, the phosphorylation state of its intrinsically disordered cytosolic domain determines whether PAM is returned to the secretory pathway or subjected to intramembrane proteolysis, generating a short-lived soluble fragment of its COOH-terminal domain (sfCD) that can accumulate in the nucleus, affecting gene expression (12).

Using a corticotrope tumor cell line in which PAM expression can be induced upon exposure to doxycycline [induced PAM (iPAM) cells], we previously demonstrated that increased expression of PAM causes rearrangement of the actin cytoskeleton, diminishes the proteolytic processing of precursors, forces secretory products to accumulate in the *trans*-Golgi, and dampens the ability of cells to respond to secretagogues (13). Microarray analysis identified a set of almost 2000 genes whose expression was up- or downregulated in concert with the 40- to 100-fold increase in PAM expression that occurred within 48 hours of treatment with doxycycline (14). Strikingly, reducing the expression of PAM in *C. reinhardtii* affects similar functions, including Golgi morphology, secretion of specific proteins, and organization of the actin cytoskeleton. More important, a reduction in PAM expression impairs ciliogenesis in a vast range of evolutionarily distant species, including *C. reinhardtii*, *Schmidtea*, and mouse (5, 7).

The presence of PAM in the ciliary membranes of *C. reinhardtii* suggests that this enzyme has an ancient role in detecting and responding to environmental stimuli. PAM requires molecular oxygen along with ascorbate, copper, and zinc, and peptide amidation is as sensitive to hypoxia as hypoxia-inducible factor (HIF) 1α (15). Consistent with this idea, PAM expression in endothelial cells (16, 17) and in several tumor cell lines is induced by hypoxia (Gene Set Enrichment Analysis; Broad Institute). These new insights into PAM function prompted us to undertake a more detailed exploration of changes in gene expression associated with altered expression of PAM in iPAM AtT-20 cells using global RNA sequencing (RNA-seq) (6, 18). Our hypothesis was that identification of genes whose expression responded to changes in PAM expression would reveal fundamental pathways not currently recognized as major contributors to the control of peptide secretion.

Materials and Methods

Cells

The AtT-20 corticotrope tumor line with doxycycline-inducible expression of rat PAM was maintained and induced as described (13); briefly, identical wells of cells were maintained in DMEM-F12 with penicillin-streptomycin, 25 mM HEPES, and tetracycline-free fetal bovine serum. PAM expression was induced by adding 4 μg/mL doxycycline to the medium; induction of PAM expression (by ~100-fold, to the level observed in rat and mouse pituitary and heart) was verified by PAM enzyme assay, Western blot, and quantitative PCR (qPCR). We also compared gene expression in wild-type (Wt) AtT-20 cells to gene expression in two stably transfected clonal AtT-20 lines expressing rat PAM-1; one line was generated using a pCI.neo vector (called AtT-20/PAM cells), and one was generated using a pCIS vector (called AtT-20/PAM* cells) (13, 19–21). Both lines express PAM at the same level as fully induced iPAM cells.

Primary anterior pituitary cultures were prepared from adult mice and rats (an approximately equal mixture of males and females) as described (22). In secretion studies, anterior pituitary and AtT-20 cells were maintained in complete serum-free medium [CSFM; DMEM/F12, penicillin-streptomycin, 25 mM HEPES, insulin-transferrin-selenium (Life Technologies, Cambridge, MA)] (22), which supports their long-term growth, or in HEPES-saline-glucose (in mM: NaCl, 137; $CaCl_2$, 2; $MgSO_4$, 1; KH_2PO_4, 0.5; glucose, 5.55; HEPES, 15; pH 7.35), similar to solutions often used in studies of secretion and in electrophysiological slice recordings. Secretion was stimulated using 1 mM $BaCl_2$, 1 μM phorbol-myristate acetate, or 20 or 40 nM corticotropin-releasing hormone ($Met^{21}His^{32} \rightarrow Nle^{21}Tyr^{32}$; Phoenix Pharmaceuticals, Burlingame, CA). As a control, purified rat PAM Exon 16 Protein (105 residues) was added for 1 hour to confluent AtT-20 cells in CSFM and HEPES-saline-glucose (HSG) as a test of peptide stability after secretion into the medium; the exogenous exon 16 protein was all recovered intact from CSFM and from HSG (not shown). We previously demonstrated the stability of POMC products after secretion (23). Our mouse studies were approved by the University of Connecticut Health Center Institutional Animal Use and Care Committee.

RNA-seq

RNA was extracted and purified as previously described (24). RNA-seq was performed on barcoded libraries, eight samples per lane, using 76-nt paired-end reads. The result was

an average of 16.6 million reads per sample, followed by Bowtie and Cufflinks alignment (https://bioinformatics.uconn.edu/software/) to identify transcripts (*Mus musculus* genome mm10, NCBI Build 38, 2011, allowing zero mismatches; http://bowtie-bio.sourceforge.net/manual.shtml); 70% to 78% of the reads aligned to known transcripts, as expected after removal of rRNA (25). Many studies recommend filtering out genes with low expression to improve discovery of truly differentially expressed genes, so genes with fragments per kilobase of transcript per million mapped reads (FPKM) <1 were excluded (25, 26). In addition, transcripts with outliers beyond 30% to 50% of the mean for the treatment group were eliminated (25–27). As recommended, analyses of differential expression were performed with three different analytical packages: Cuffdiff (https://bioinformatics.uconn.edu/software/), Limma (http://genexplain.cam.uchc.edu:8080/bioumlweb/), and DESeq2 (CGI Storrs; http://bioinformatics.uconn.edu/). As expected (25, 26, 28–30), a much higher number of apparently differentially expressed genes were identified using Cuffdiff than with Limma or DESeq2, suggesting a higher false discovery rate for Cuffdiff (25, 26, 28–31). Repeating the analyses after deleting the upper quartile of transcripts (30, 32) did not materially alter the results. Because of the close similarity at the nucleotide level between endogenous mouse PAM and exogenous rat PAM, 76-nt reads could not always distinguish the two transcripts. Because rat PAM is induced >100-fold by doxycycline, we dropped PAM from the list of regulated transcripts. The FPKM values and lists of differentially expressed genes are in Supplemental Table 1 and Supplemental Fig. 1. The primary sequencing data have been deposited in the Gene Expression Omnibus under the series record number GSE110809.

Pathway analyses

Data were analyzed through the use of Ingenuity Pathway Analysis (IPA; Qiagen Germantown, MD). Because DESeq2 and Limma have high false-negative rates, we combined the two lists for pathway analysis. Many of the transcripts identified by Cuffdiff as differentially regulated had high variances. To eliminate these, we included only the 320 transcripts with a CuffSig value <0.4 [Eq. (1)]:

$$\text{CuffSig} = \text{Abs}([\text{Stdev(Basal)} + \text{Stdev(Induced)}]/[(\text{Average(Basal)} - \text{Average(Induced)})]).$$

Approximately 50% of the Cuffdiff transcripts meeting this criterion were in the DESeq2 + Limma pool already, so the net pool of transcripts analyzed using IPA was 444, a number within the recommended range of 100 to 3000 transcripts. One of the transcripts verified by Western blot and qPCR (see below) was identified only in this CuffSig pool (Fkbp2), not by DESeq2 or Limma.

qPCR validation

For validation, new sets of AtT-20 iPAM cells were grown as above, and new samples of RNA were prepared, followed by cDNA synthesis and qPCR using the primers listed in Table 1. RNA was also prepared from AtT-20/PAM and AtT-20/PAM* cells. All primers had calculated melt temperatures of 60°C to 62°C, and all products were 120 to 130 bp in length, as verified by agarose gel electrophoresis (24). The qPCR program was 95°C, 3 minutes; 95°C, 10 seconds; 55°C, 15 seconds; and 72°C, 40 seconds, repeating the second and fourth steps 39 more times. Maximal stepwise amplification ratios (at the midrange during maximal signal amplification) were 1.8 or greater for all primer sets. The initial cDNA preparation and qPCR kits from BioRad (Hercules, CA) were used as described (24), along with the GoScript Reverse Transcription Mix (Random Primer) and GoTag qPCR Master Mix, both from Promega (Madison, WI).

Protein levels were evaluated in SDS lysates prepared from Wt and two stably transfected AtT-20 lines (PAM and PAM)*

Independent cell lysates (n ≥ 11 for each type of cell line) were prepared by extracting cells into SDS-P lysis buffer (1% SDS, 50 mM Tris, 130 mM NaCl, 5 mM EDTA, 50 mM NaF, 10 mM Na pyrophosphate, pH 7.6) containing 1 mM Na orthovanadate, 1 mM phenylmethylsulfonyl fluoride, and protease inhibitor cocktail (33). After heating at 95°C for 5 minutes, samples were sonicated and insoluble material was removed by centrifugation at 16,000*g* for 20 minutes at room temperature. Protein levels were determined using the bicinchoninic acid assay (Thermo Scientific, Waltham, MA) with bovine serum albumin as the standard, and aliquots containing equal amounts of protein (generally 30 μg) were analyzed pairwise on 4% to 15% gradient gels (Criterion TGX; BioRad). After transfer to a polyvinylidene difluoride membrane, immunoblots were visualized using SuperSignal West Pico PLUS Chemiluminescent substrate (Thermo Scientific). Images were quantified using a SynGene Pxi4 imaging system, with images in the linear range. Intensities were calculated with respect to nearest neighbor Wt samples to adjust for any variation across the gel. Bars in graphs represent 6 to 15 ratios, mean ± SEM. For differentially expressed transcripts of interest, available antibodies were used to probe the entire length of the gel; patterns were compared with the predicted molecular weight and to publications using that antiserum. Antibodies used included the following: ATF3 (D2Y5W; catalog no. 33593; Cell Signaling (Danvers, MA); RRID: AB_2195171), ATG9B (NBP1-77169; Novusbio, Littleton, CO; RRID: AB_11004885), CD68 (25747-1-AP; Proteintech, Chicago, IL; RRID: AB_2721140), Cystatin C (EPR4413; ab109508; Abcam, Cambridge, MA; RRID: AB_10888303), FKBP2 (11700-1-AP; Proteintech; RRID: AB_2102876), FKBP4 (10655-1-AP; Proteintech; RRID: AB_2246853; Gapdh (clone 6C5; MAB374; Millipore, Burlington, MA; RRID: AB_2107445), rat GH(209–216) [JH89 (34); RRID: AB_2721273], PAM-Exon 16 [JH629 (35); RRID: AB_2721274], POMC–16K [Georgie (36); RRID: AB_2721275], POMC-γ_3MSH [JH189 (37); RRID: AB_2721276], PRL (catalog no. AF1445; R&D Systems, Minneapolis, MN; RRID: AB_2170970), SEC61B (catalog no. 15087-1-AP; Proteintech; RRID: AB_2186411), PAI1 (Serpine1; ab7205; Abcam; RRID: AB_305758), PAI1 (Serpine1; catalog no. 13801-1-AP; Proteintech; RRID: AB_2186881), Tubb3 [TUJ1 (class III β-tubulin) antibody; TUJI, Covance, Hazelton, PA; MMS-435P; RRID: AB_2313773], TXNIP (D5F3E; catalog no. 14715; Cell Signaling; RRID: AB_2714178), BSG (11989-1-AP; Proteintech; RRID: AB_2290597), CHAC1 (LS-C353541-100; LSBio, Seattle, WA; RRID: AB_2721141), REDD1 (Ddit4; ab106356; Abcam; RRID: AB_2245711), DDIT4 (ab106356; Abcam; RRID: AB_10864294), Hilpda (HIG2; sc-376704; Santa Cruz, Dallas, TX; RRID: AB_11149940), Myotilin (MYOT; LS-C482611-50; LifeSpan BioSciences, Seattle, WA; RRID: AB_2721142), and Ndrg1 (D8G9-XP; catalog no.

Table 1. iPAM Primer Composite

Transcript	Forward	Reverse
Adm	AAGGCTATGGCCGCCGGCG	AAGAGTCTGGAGATGTGCGCCCAG
Atf3	GATATACATGCTCAACCTGCACCGGC	CCTCTGCTTAGCTCTGCAATGTTCCTTC
Atf5	CACAGCAGCCTCCTCCTCTGG	ACTTATTCTGGTCTCTCTTCTTTTGCTTGCG
Atg9b	AGGAGGCACAGGGGGCCAGAAG	TCTCCCCATAGTTCTTGCTGCTGCTG
Bsg	TGTTGACCCTGGCACCTACGTGTG	AGCCACGATGCCTAGGAAGGGC
Btg2	ATCGCCGCCGCCGTGGGTTT	TGGTGTTTGTAATGATCGGTCAGTGCGTC
Cck	GAAGCTACGGACCCCGTGGAG	GATGTATCGCGCTAGCAGTGCGC
Cd68	AAAGCTTCTGCTGTGGAAATGCAAGCATAG	GAAACATGGCCCGAAGTGTCCCTTG
Chac1	CTCCTGAAGAGGTCATTGCCACACAG	CTCATCTTGTGCCTGAGGCCCACA
Ddit4	GGTGCCCACCTTTCAGTTGACCC	TCAGGGACTGGCTGTAACCAGGG
DFosb[a]	GAGCTGCAAAAAGAGAAGGAACGCCTG	GAGGACTTGAACTTCACTCGGCCAG
Dusp1	AAGTGCTAGCCCCTCACTGCTCTG	TCGTGGGGTGGACGGGGATG
Fkbp2	GTGAAGGGGAAAAGCGGAAGTTGGTG	CAATCTTGAGCAGCTCCACCTCAAACAC
Fkbp4	CTCGCCCGGGAAAAGAAGCTCTATG	CTCACCCTTCATCTCAGCATCAGTGG
Fkbp5[a]	CCAGAGGAAGGCGAAGGAGCACAA	ACAGCCTTCTTGCTCCCAGCTTTGCTGGC
Fos[a]	GTCACCTGTACTCCGGGCTGC	CTCGTTGCTGCTGCTGCCCTTTC
Fosb[a]	GAGAGATTTGCCAGGGTCAACATCCG	GCCGTCAGGTTGGGGGGTGC
Gipr	GCTGCTTCTGCTGCTGTGGTTGTG	ATCTTTTGGCACTCCTGGCCGTAGTG
Hif1a	ATATCTAGTGAACAGAATGGAACGGAGCAAAAG	AATCGTAACTGGTCAGCTGTGGTAATCC
Hilpda	AGAGTGATGGAGTCTCTGGGAGGC	TCGGGATGGATGGTCTGGCAGG
Hpd	TCGACTATGACGAGAAAGGCTACCTCC	AGTTGCCCGCTCCAAAGCCCTG
Hprt	GACTGAAAGACTTGCTCGAGATGTCATG	AGTGCTTTAATGTAATCCAGCAGGTCAGC
Ift20	GAAGCAGAGAACGAGAAGATGAAGGCC	TGCGTCTTCTTTTCTGCTATCAGGGCC
Insrr[a]	TGGATCGCATACAGGATGAGCTTCGG	GTGGGGAATCAGGTTCTGCCTCAGTA
Kcnab2[a]	CAGGAATCTGGGCAAATCTGGCCTTC	TTATCGTAGGCCAAGGTCATTAGGTGC
Kcnk16[a]	CTCCTAGGACTGGCATGGCTGG	GTCAGGGGCTGCTCCATCCTTAAG
Lamb1	GGCTCAAGCTAACAGCAAGCTCCAG	GAGCGAACCTCTCCTTCCAGTCG
Lamb3	AGAGGAGCTCTTTGGGGAGACCATG	CTTCTCCAGCCCCGACAGGTCTG
Myot	TAAGCAGCTGCGTGTTCGACCAACATTC	CCGGATTGAGCTGCCAGGCG
Ndrg1	TACCAGCGAGGGCCCCCGAAG	GCATTGTTTCCGGTGGCACCCGA
Nr1d1	AGCAGCTCCAGGAGACGCTGCT	TTGTTCAGGGTCCGCAGGTCCG
Ppia	TTCCAGGATTCATGTGCCAGGGTGG	TGCCAGGACCTGTATGCTTTAGGATGAA
Ppp1r16b[a]	ATCGCAAGCGCAAGCATGAGCGG	AACCTTGTTCTTCAGGAAGTAGCGAACTTC
Ppp1r3c[a]	CCACGTCCTTTGACAAGTTCCGTCATG	AAAATTTCTTCGTTGAAAACCATTGTAAGGACCC
Psph	AGAAAATAATCATGATTGGAGATGGAGCTACGG	ACCACTTGGCGTTGTCCTTAACCTGC
R3hdml[a]	CTGGTCTGCAACTACGCCATTAAGGG	GAAGCACATGTTGCTGTTGCAGTTGCC
ratPAL	GAGTCCTCTGGAAGCAGTCCTAGG	GAAGCATTGGATTCGGCCATTTTCCCTG
ratPHM	GACCAGTCACCCCTCTTGATGCATC	AGGCTTCCTCATCCACAGGCAGAC
Rgs9	ACGGGAGTCAGAATGCATAACCAGAGAG	ACAATAAAGTTGCCCAGGTTCTGTGCC
Rplp1	AGGTGACGGTCACGGAGGATAAGATC	TGAGGCTCCCAATGTTGACATTGGCC
Sat1	TCTTGGTAGCAGAATGGAATGAACCATCTATCA	CATTTTTAGCAAGTACTCTTTGTCAATCTTGAAGAG
Sdha	CTCTTGGACCTTGTAGTCTTTGGCAGAG	AAGATTCATAACCGATTCTTCTCCAGCATTTGC
Sec61b	CACCTCTGCAGGGACTGGGGG	AGCATAAATACAGCAGCGATGAACAGAAGAC
Serpine1	TCTGGAGACTGAAGTGGACCTCAGAG	CCTGTGCTACAGAGAGCTGCTCTTG
Slc26a10[a]	GAAGTGGTCCAGCTCACCAGGC	TGGAGACACGCTATCCAGGAGTCTC
Sln	GTTCTCATCCAGACATTCTGAAGATGGAGA	CTCAGTATTGGTAGGACCTCACGAGG
Sprr1a	CTTGTGCCCCCAAAACCAAGGATCC	AGGGCTCAGGTGCCTTGGGGTGG
Tubb3	AACAGCAGCTACTTCGTGGAGTGGATC	AACAGCTCCTGGATGGCCGTGC
Txnip	CTCTGCTGGACGATGTGGACGAC	ACAGGGTGGCAGGGCTCAGGC
Unc5cl[a]	GAGCTGCACTATCTCATGACCTCCATG	GTTCTCCCAGGTGCCTCCATGCAA

All melt temperatures 60°–62°C; 120–130 nt products.

[a]Low expression, or data too variable among biological replicates.

9485T; Cell Signaling; RRID: AB_2721143). Of the 21 antisera tested, 15 passed this quality control test (bands where expected, no bands where not expected).

Results

Basal or constitutive secretion includes newly synthesized secretory proteins released as soon as they traverse the Golgi complex. Endocrine cells store a subset of their newly synthesized luminal proteins in secretory granules for rapid release in response to specific secretagogues (stimulated secretion). Although changes in cargo protein synthesis affect both basal and stimulated secretion, these changes require more time than does altering the rate of secretory granule exocytosis alone.

Stimulated secretion is altered by nutrients/growth factors and by PAM

The POMC products released by pituitary corticotropes provide a sensitive means of comparing basal to stimulated secretion; products stored in secretory granules respond to corticotropin-releasing hormone (CRH), whereas larger precursors and biosynthetic intermediates do not (18). Corticotrope secretion was assessed using an antibody to the *N*-terminal region of POMC (16K fragment); this antibody cross-reacts with the larger POMC products that contain the 16K fragment (Fig. 1A). To facilitate the analysis of POMC products released into the medium, CSFM was used for these studies. Both primary pituitary cells and AtT-20 cells can be maintained in CSFM, which contains insulin, transferrin, and selenium, for months (22). Basal CSFM contained small amounts of POMC and the 16K fragment. In response to CRH, secretion of the 16K fragment rose about fourfold, with little increase in the release of larger POMC products.

To determine whether nutrient/growth factor availability affected the ability of pituitary corticotropes to respond to CRH, pituitary cells were incubated for 1 hour in HSG instead of CSFM; after a 1-hour collection of basal media (CSFM or HSG), cells were incubated for

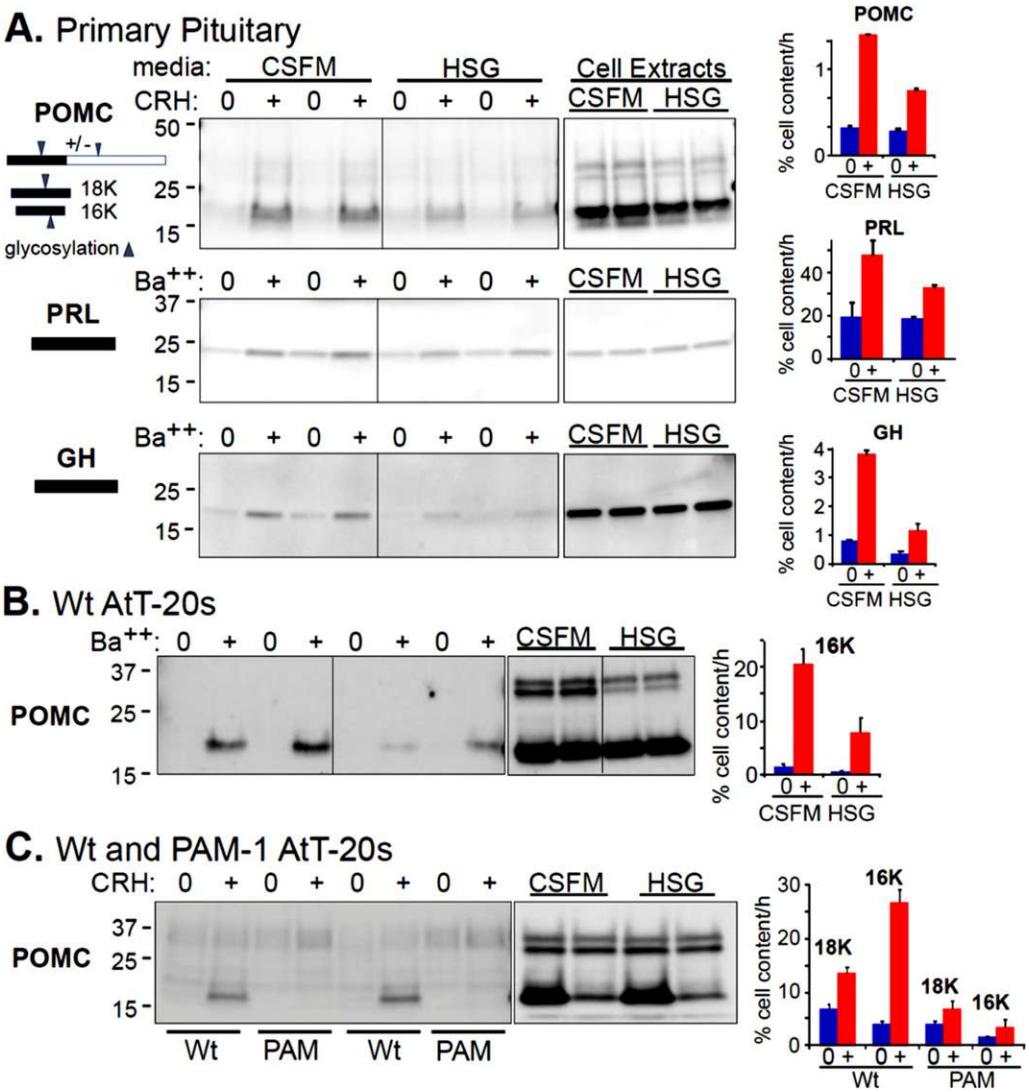

Figure 1. Pituitary secretion is sensitive to nutrient/growth factor status. (A) Primary mouse anterior pituitary cultures were maintained in CSFM (DMEM/F12 with insulin, transferrin, and selenium) for 48 h and then incubated in duplicate in CSFM or HSG for 1 h (basal) and then 1 h (stimulated) with either 1 mM $BaCl_2$ or 40 nM CRH. Cells were extracted in SDS-lysis buffer, boiled, and sonicated. Aliquots of media and cell extracts were subjected to Western blot analysis using antisera to POMC (16K fragment), GH, or prolactin (PRL) (Table 2). Data were quantified (as percentage of cell content secreted per hour) on a Pxi4 digital imaging analysis system using GeneTools (Syngene). Similar results were obtained from two additional sets of mouse anterior pituitary cultures and one set of rat anterior pituitary cultures. (B) Wt AtT-20 mouse corticotrope tumor cells were treated and analyzed as in (A), using $BaCl_2$ as stimulant and γ_3MSH antiserum for Western blot analysis. (C) Secretion of POMC products was assessed in Wt and AtT-20/PAM cells incubated for sequential 1-h time periods with CSFM and CSFM containing 40 nM CRH, after which cell lysates were prepared and Western blot analyses performed with 16K fragment antiserum. + CRH, response to corticotropin-releasing hormone; 0 CRH, basal complete serum-free medium.

an additional 1 hour in CSFM or HSG containing a maximally effective dose of CRH, and cell extracts were prepared (Fig. 1A). Strikingly, the ability of corticotropes to release the 16K fragment in response to CRH was reduced by a factor of 2 when cells were incubated in HSG.

We next wanted to know whether this brief lack of nutrients/growth factors had a similar effect on the stimulated secretion of prolactin and GH; $BaCl_2$, which mimics increased cytosolic calcium levels in many cell types (38, 39), was used to stimulate both lactotropes and somatotropes (Fig. 1A). In CSFM, secretion of prolactin was stimulated about twofold by $BaCl_2$, and secretion of GH was stimulated about fivefold (as observed for POMC products). For both lactotropes and somatotropes, the ability of $BaCl_2$ to stimulate hormone secretion was diminished below 50% of control when cells were incubated in HSG instead of in CSFM.

The AtT-20 corticotrope tumor cell line has served as a simple, homogeneous model system for investigating pituitary hormone secretion. As for primary corticotropes, when incubated in CSFM, $BaCl_2$ stimulated the secretion of the 16K fragment by Wt AtT-20 cells without affecting POMC secretion (Fig. 1B). Incubation of Wt AtT-20 cells in HSG instead of CSFM markedly decreased the amount of the 16K fragment secreted in response to CRH, as observed for pituitary corticotropes.

AtT-20/PAM cells stably express rat PAM-1 at levels similar to those observed in pituitary and heart (20, 33). Reducing the expression of PAM in *C. reinhardtii*, which relies on basal secretion but is not known to store products in secretagogue-sensitive granules, inhibited the secretion of selected proteins (7), suggesting a role for PAM in basal secretion. Elevated basal secretion of POMC products was previously demonstrated in AtT-20/PAM cells (20); the ability of Wt and AtT-20/PAM cells to respond to CRH with increased secretion of POMC products was compared (Fig. 1C). As expected, when incubated in CSFM, secretion of the 16K fragment by Wt AtT-20 cells increased over fivefold. PAM-1 expression in AtT-20 cells blunted the ability of CRH to stimulate secretion (Fig. 1C); a similar inhibitory effect of PAM-1 on stimulated secretion was reported earlier for $BaCl_2$ (13). Expression of exogenous PAM-1 in primary pituitary cells was previously shown to blunt their ability to respond to secretagogue (33). Based on these observations, AtT-20 cells can serve as a simple model for the effects of nutrients/growth factors and PAM on stimulated secretion.

Basal secretion is altered by nutrients and by PAM

To better evaluate the role of PAM in basal secretion, POMC release by Wt and PAM-1 AtT-20 cells was evaluated over longer times. Wt cells released small amounts of intact POMC, the 18K fragment and 16K fragment (Fig. 2A). In contrast, PAM-1 cells released large amounts of intact POMC, ACTH, ACTH biosynthetic intermediate, and the 18K fragment (Fig. 2B). To assess the role of nutrients/growth factors in basal secretion, the cells were incubated in CSFM or in HSG (Fig. 2A and 2B). Strikingly, for both Wt and AtT-20/PAM cells, incubation in HSG greatly reduced the basal secretion of POMC products.

Our earlier array analysis (14) identified multiple genes whose expression was regulated in response to increased expression of PAM-1 in AtT-20 cells. Knowing that the stimulated and basal secretory pathways in corticotropes were rapidly affected by a lack of nutrients/growth factors, we decided to return to our inducible system and take advantage of the specificity and sensitivity afforded by RNA-seq analysis to improve upon our earlier array analysis (14).

RNA-seq analysis of basal and induced iPAM AtT-20 cells

Based on our previous studies, 2 days of growth in medium containing doxycycline increases PAM-1 expression in iPAM AtT-20 cells 100-fold (13). Of 23,351 transcripts analyzed, 11,872 had values high enough to merit analysis (basal and induced FPKM values both

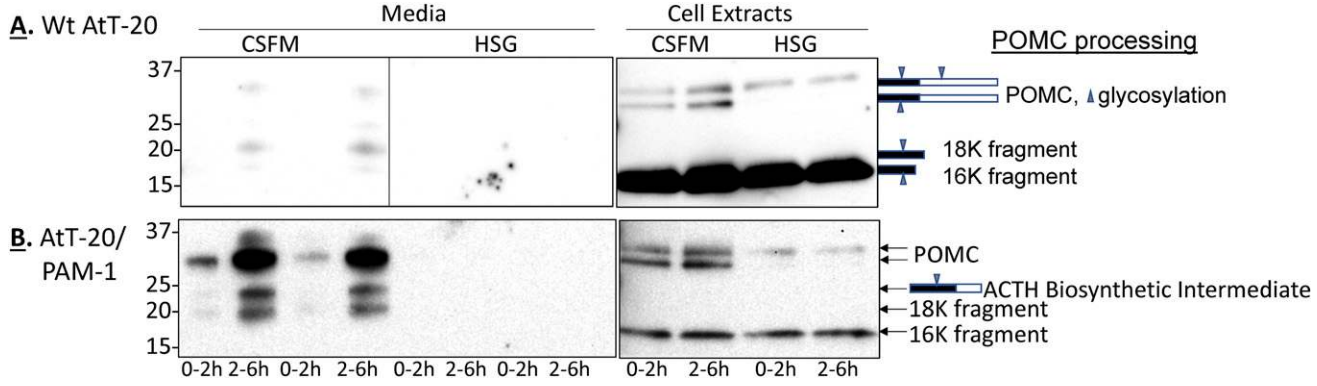

Figure 2. Corticotrope basal secretion is sensitive to expression of PAM-1. (A) Wt AtT-20 cells and (B) AtT-20/PAM cells were incubated in CSFM or HSG for sequential time periods (0 to 2 h and 2 to 6 h), after which cell lysates were prepared. POMC products were detected by Western blot analysis of cell extracts and spent media using the 16K fragment antibody. POMC product terminology is illustrated in the diagram.

above zero and at least one FPKM value ≥1). A histogram showing the induced/basal FPKM ratios for these 11,872 genes indicated that downregulation was a more common response to PAM expression than upregulation. Among the transcripts exhibiting the greatest fold change, three-fourths were decreased.

We used several different programs to identify differentially expressed genes that withstand accepted statistical tests. Cuffdiff analysis identified 1548 differentially expressed genes [6.5% of the mouse genome (Supplemental Table 1)], with levels of one-third of these transcripts increasing and two-thirds decreasing in response to increased PAM expression (Fig. 3B); Limma identified only 145 differentially expressed genes and DESeq2 identified 195 (Fig. 3B). Of these targets, 58 differentially regulated genes were identified by both Limma and DESeq2, and 56 of these were also identified by Cuffdiff. These genes, along with others of interest that were further analyzed, are listed as transcripts of interest in Table 2. Only two transcripts in the 3× up group and eight in the 3× down group in Fig. 3A survived statistical scrutiny to be in Table 2; none of the transcripts in the 10× up or down groups (except rat PAM) are in Table 2.

This type of discrepancy between analytical methods, which has been reported in multiple studies (28), led us to use a stepwise approach to exploring our RNA-seq data. For qPCR validation, analyses were generally limited to transcripts of interest with FPKM values above 10; over half of these transcripts were tested by qPCR. Transcripts of interest were also examined in Wt AtT-20 cells and in two stable AtT-20/PAM lines, followed by Western blot analysis. Finally, pathway analysis was used to identify pathways not currently known to affect secretion, testing our initial hypothesis.

qPCR validation of RNA-seq data and extension to Wt vs AtT-20/PAM cell lines

For qPCR, a crucial choice is the reference transcript (40–42). Glyceraldehyde 3-phosphate dehydrogenase (Gapdh), a commonly used reference transcript, appeared in the list of differentially regulated transcripts (Table 2). The FPKM data for the iPAM cells were used to decide among several other commonly used reference genes: β-actin (Actb), peptidylprolyl isomerase A (Ppia), succinate dehydrogenase subunit a (Sdha), hypoxanthine guanine phosphoribosyl transferase (Hprt), and two large ribosomal proteins (Rplp0 and Rplp1). The coefficient of variation was lowest (<10%) for Ppia and reached levels as high as 21% for Gapdh and 23% for Rplp0.

To validate the RNA-seq data, over half of the transcripts identified by one or more differential expression analysis tools (Table 2) were subjected to qPCR analysis. Induced/basal ratios based on qPCR analysis and FPKM data were compared (Fig. 4A). For 34 transcripts, nearly 90% of the transcripts fell into the first and third quadrants: increased in both RNA-seq and qPCR data or decreased in both RNA-seq and qPCR data; the best-fit line had a slope of 0.79 and $R^2 = 0.53$. As controls, qPCR product sizes (120 to 130 nt) were each verified by gel analysis; peak amplification per PCR cycle exceeded 1.8-fold for each of these transcripts. In cases where the identity of the transcript could be questioned, because of possible confusion from closely related genes (such as for Tubb3, β3-tubulin), the PCR product was isolated and sequenced. Data failing to meet all of these criteria were excluded from this comparison.

Our RNA-seq data identified transcripts whose abundance changed within 48 hours of exposure to doxycycline; PAM expression in these cells would have

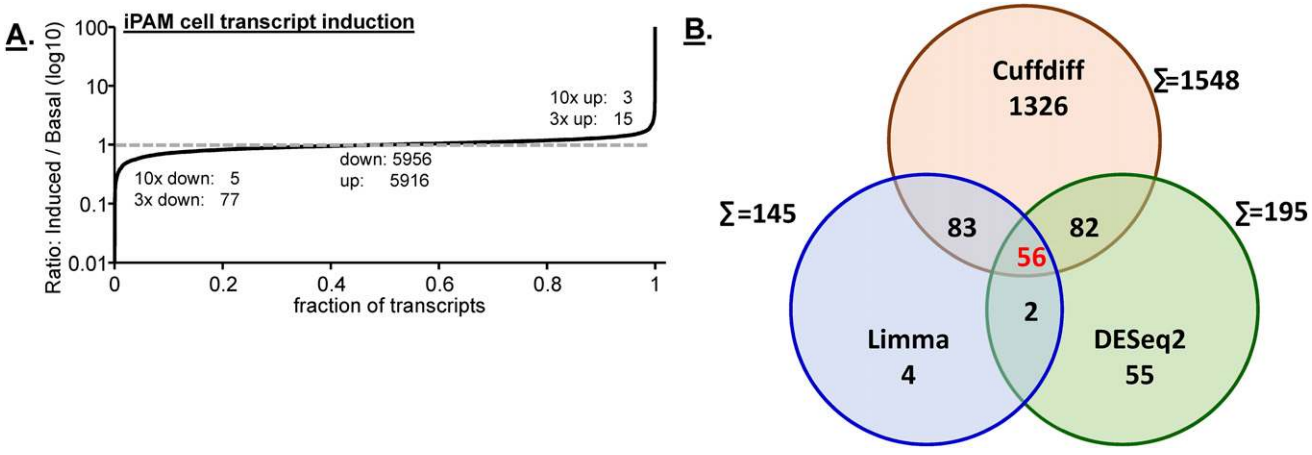

Figure 3. Differential gene expression in doxycycline-induced iPAM AtT-20 cells. (A) The 11,872 transcripts for which the average FPKM value was above 0 for both basal and induced samples and above 1.0 for at least 1 of the 2 samples were ranked by induced/basal ratio. (B) RNA-seq analysis of triplicate RNA samples prepared from iPAM AtT-20 cells before and after doxycycline induction of PAM expression (48 h of doxycycline exposure) used Cuffdiff, Limma, and DESeq2: for Cuffdiff, $q < 0.05$; DESeq2, $P < 0.05$; Limma, $B > 0$. Although 56 differentially expressed genes were identified by each program, many transcripts were identified only by a single program.

Table 2. Transcripts of Interest

Name	Description (From MouseMine Blog, Jackson Laboratory, Bar Harbor, ME)	FPKM Mean	Log2 Induced/ Basal	Hypoxia Responsive
Lower transcript abundance in iPAM cells				
Tnfrsf9	Tumor necrosis factor receptor superfamily, member 9	13	−2.5	[a]
Cd68	CD68 antigen	4	−2.4	[a]
Fam71f2	Family with sequence similarity 71, member F2	7	−2.3	
Kcnab2	Potassium voltage-gated channel, shaker-related subfamily, β member 2	4	−2.0	
Myc	**Myelocytomatosis oncogene**	**8**	**−2.0**	[a]
Sprr1a	Small proline-rich protein 1B	307	−1.7	
Pglyrp1	Peptidoglycan recognition protein 1	11	−1.8	
St3gal1	ST3 β-galactoside α-2,3-sialyltransferase 1	15	−1.9	
Rgcc	**Regulator of cell cycle**	**14**	**−1.7**	
Lamb3	Laminin, β3	16	−1.6	[a]
Lamb1	Laminin B1	4	−1.5	
Ppp1r16b	Protein phosphatase 1, regulatory (inhibitor) subunit 16B	11	−1.5	
Plk2	Polo-like kinase 2	95	−1.5	[a]
Fos	**FBJ osteosarcoma oncogene**	**32**	**−1.4**	[a]
Ppp1r3c	Protein phosphatase 1, regulatory (inhibitor) subunit 3C	64	−1.4	[a]
Cck	Cholecystokinin	30	−1.3	
Smox	Spermine oxidase	6	−1.2	[a]
Lmcd1	LIM and cysteine-rich domains 1	63	−1.2	
Etv5	**Ets variant 5**	**24**	**−1.2**	
Maff	**v-maf musculoaponeurotic fibrosarcoma oncogene family, protein F (avian)**	**60**	**−1.1**	[a]
Hilpda	Hypoxia-inducible lipid droplet associated	137	−1.1	
Adm	Adrenomedullin	75	−1.1	[a]
Atf3	**Activating transcription factor 3**	**121**	**−1.1**	[a]
Bhlhe40	**Basic helix-loop-helix family, member e40**	**158**	**−1.0**	[a]
Nr1d1	**Nuclear receptor subfamily 1, group D, member 1**	**77**	**−1.0**	[a]
Ddit4	DNA damage-inducible transcript 4	1210	−1.0	[a]
Serpine1	Serine (or cysteine) peptidase inhibitor, clade E, member 1	211	−1.0	[a]
Txnip	Thioredoxin interacting protein	415	−1.0	[a]
R3hdml	R3H domain containing-like	32	−1.0	
Dusp1	Dual-specificity phosphatase 1	55	−1.0	[a]
Btg2	**B-cell translocation gene 2, antiproliferative**	**261**	**−1.0**	[a]
Dcxr	Dicarbonyl L-xylulose reductase	54	−0.9	
Bbc3	BCL2 binding component 3	105	−0.9	
Rgs9	Regulator of G protein signaling 9	67	−0.8	
Pnrc1	**Proline-rich nuclear receptor coactivator 1**	**197**	**−0.8**	[a]
Atg9b	Autophagy-related 9B	24	−0.8	[a]
Mybl1	Myeloblastosis oncogene-like 1	69	−0.7	
Zfand2a	Zinc finger, AN1 type domain 2B	64	−0.7	
Gipr	Gastric inhibitory polypeptide receptor	57	−0.7	
Tor4a	Torsin family 4, member A	79	−0.6	
5430416N02Rik	RIKEN cDNA 5430416N02 gene	95	−0.6	
1810032O08Rik	RIKEN cDNA 1810032O08 gene	89	−0.6	
Elf3	**ETS-related transcription factor Elf-3**	**212**	**−0.5**	[a]
Sat1	Spermidine/spermine N1-acetyl transferase 1	248	−0.5	[a]
Bsg	Basigin	4681	−0.5	
Ndrg1	*N*-myc downstream regulated gene 1	626	−0.4	[a]
Gpi1	Glucose phosphate isomerase 1	1357	−0.3	
2410006H16Rik	RIKEN cDNA 2410006H16 gene	397	−0.3	
Higher transcript abundance in iPAM cells				
Fkbp2	FK506 binding protein 2	57	0.5	
Ift20	Intraflagellar transport 20	80	0.7	
Gapdh	Glyceraldehyde-3-phosphate dehydrogenase	7107	0.7	
Gm10845	Predicted gene 10845	116	1.1	

(*Continued*)

Table 2. Transcripts of Interest (Continued)

Name	Description (From MouseMine Blog, Jackson Laboratory, Bar Harbor, ME)	FPKM Mean	Log2 Induced/ Basal	Hypoxia Responsive
Fkbp4	FK506 binding protein 4	178	1.1	[a]
Sec61b	Sec61 β subunit	251	1.1	
Tmem179	Transmembrane protein 179	72	1.2	
Psph	Phosphoserine phosphatase	140	1.3	
Atf5	**Activating transcription factor 5**	**230**	**1.3**	
Tubb3	Tubulin, β3 class III	211	1.3	
Rangrf	RAN guanine nucleotide release factor	69	1.4	
Chac1	ChaC, cation transport regulator 1	87	1.4	[a]
Spin2	Spindlin family, member 2D	12	1.5	
Cmklr1	Chemokine-like receptor 1	58	1.5	
Myot	Myotilin	58	1.5	
Sln	Sarcolipin	170	1.6	
Unc5cl	Unc-5 family C-terminal like	1	1.7	
Ffar2	Free fatty acid receptor 2	16	1.7	
Prrt3	Proline-rich transmembrane protein 3	15	1.9	
Insrr	Insulin receptor-related receptor	13	2.1	
Hpd	4-Hydroxyphenylpyruvic acid dioxygenase	7	2.7	
Kcnk16	Potassium channel, subfamily K, member 16	4	3.1	

Bold text indicates a transcription factor. The 58 transcripts identified by all three programs or by both Limma and DESeq are identified, with mean basal FPKM and the log2 induced/basal ratio shown. Based on our initial studies, each of the transcripts identified only by Limma, several transcripts identified only by DESeq2, and one transcript identified only by Cuffdiff were added to this list. The table includes a total of 70 transcripts, 48 downregulated and 22 upregulated.

[a]Hypoxia-responsive genes.

been elevated for less than 2 days. To focus on genes whose expression was responsive to the presence of high levels of PAM and not to other features unique to the iPAM cells or the rapid induction of PAM expression, we used qPCR to compare stably transfected lines expressing rPAM-1 (which exhibit similar alterations in morphology and secretory pathway function) to Wt AtT-20 cells (13). Two independent clonal lines (AtT-20/PAM and AtT-20/PAM*) created with different vectors a decade apart were used. We first used qPCR to determine whether Ppia could be used as the reference transcript (Fig. 4B); Ppia again exhibited the smallest coefficient of variation. Of the 34 transcripts tested, half exhibited a similar response in both cell systems (blue symbols in Fig. 4A). A few particularly interesting transcripts (Tubb3, Sec61b) differed between the transient PAM induction and the stable lines and were also investigated by Western blot analysis. Western blot evaluation of protein levels was attempted for >20 transcripts of interest, but antibodies with sufficient specificity and sensitivity were not always found (red symbols in Fig. 4A).

The decline in Gapdh transcript levels observed by RNA-seq after induction of iPAM cells was confirmed by qPCR analysis of RNA from induced vs basal iPAM cells and from AtT-20/PAM vs Wt lines (Fig. 4A). Western blot analyses revealed a significant decrease in Gapdh protein levels in the AtT-20/PAM* line (Fig. 4C). Gapdh and the other enzymes of the glycolytic pathway evolved well before the earliest oxygen-requiring enzymes. As part of integrating energy generation through the glycolytic and oxidative pathways, hypoxia is a potent stimulus of glycolytic flux (43). Glycolysis also occurs under normoxic conditions, with HIF-1α often playing an essential role in its regulation (44). Both *PAM* and *GAPDH* are hypoxia-responsive transcripts (Broad Institute). Of the 48 transcripts whose expression is reduced in response to PAM expression, almost half (23, or 48%) are known to be hypoxia responsive (Table 2); of the 22 transcripts whose expression is increased in response to PAM expression, 2 (9%) are hypoxia responsive. Analyses of hypoxia-responsive genes have typically identified 1% to 3% of the transcriptome in any single cell type. The enrichment of hypoxia-responsive transcripts in the set of PAM-responsive genes suggests a role for this oxygen-dependent enzyme in the response of AtT-20 cells to hypoxia.

Transcripts encoding transcription factors. Production of sfCD, the only fragment of PAM known to accumulate in the nucleus, occurs as PAM traverses the endocytic pathway in cells with and without a regulated secretory pathway (12, 45) (Fig. 5A). Current data support the presence of a well-developed endocytic trafficking pathway in the last eukaryotic ancestor (10, 11). Whether or not sfCD plays an essential role in causing the observed changes in gene expression, changes in the expression of transcription factors were of particular interest. Using IPA (Qiagen), a substantial number of the

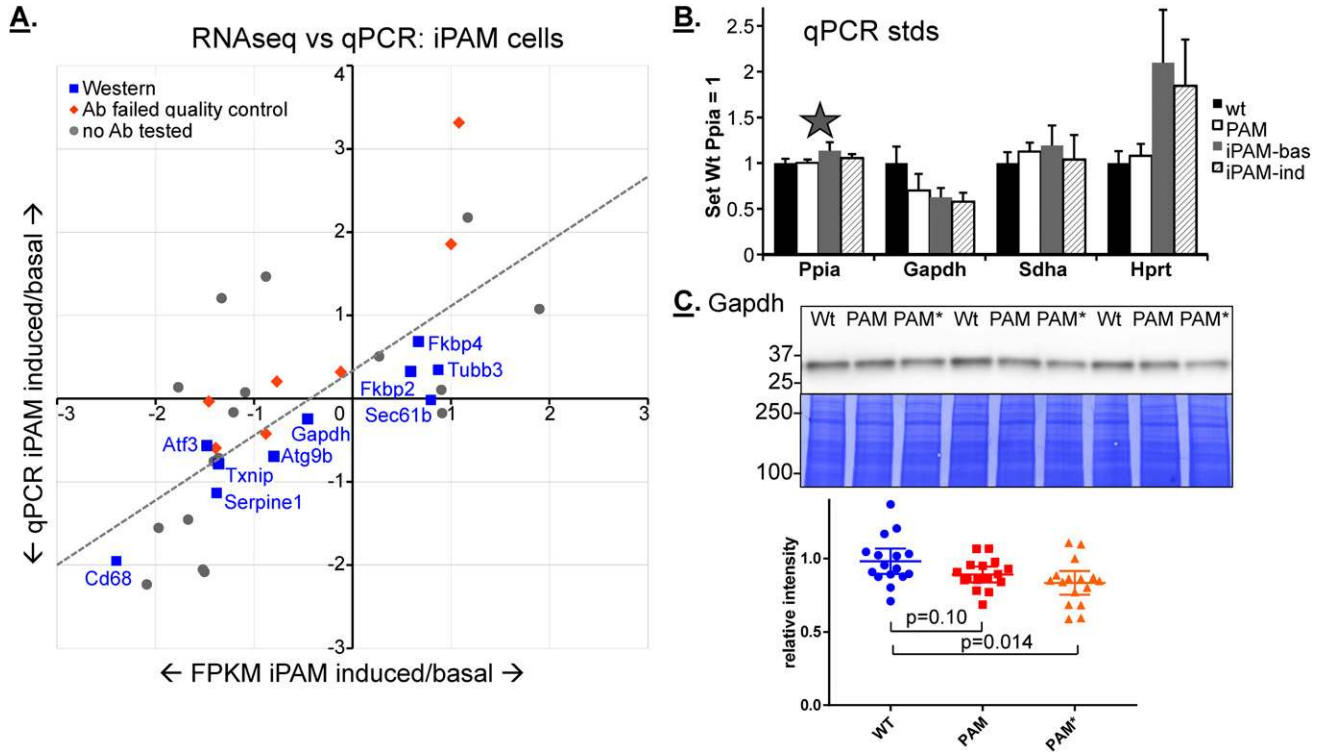

Figure 4. Validation of RNA-seq identification of differentially expressed genes. (A) RNA-seq data (FPKM ratios for induced vs basal iPAM cells) on the *x*-axis are compared with qPCR data for two independent sets of RNA samples from iPAM cells on the *y*-axis. Genes successfully evaluated using Western blots are named in blue; genes for which antibodies were obtained and tested but deemed unacceptable are indicated by red symbols; genes for which no antibody was tested are shown in gray. (B) Because our RNA-seq data identified Gapdh as a differentially expressed transcript, six genes were tested for use as an internal standard for qPCR analysis of Wt, PAM-1, and iPAM (basal and induced) AtT-20 cells; data for Gapdh, Ppia, Sdha, and Hprt are shown. (C) Lysates prepared from Wt AtT-20 cells and from two AtT-20 lines stably expressing PAM-1 (PAM and PAM*) were subjected to Western blot analysis for Gapdh. Triplicate sets of samples were analyzed; the Coomassie-stained upper part of the membrane is shown, illustrating equal loading (5 μg protein) of the different samples. Image quantification for Gapdh in Wt, PAM, and PAM* lysates was performed in the linear range of exposures, normalized by setting the average value for Wt = 1.00. Statistics, Student *t* test. Graph from Prism shows mean ± 95% CI.

differentially regulated transcripts were identified as transcription factors (Limma, 13%; DESeq2, 23%; Cuffdiff, 11%) (Table 2). We analyzed activating transcription factor 3 (Atf3), a cAMP-responsive element binding family member, because an upstream regulator, *N*-myc downstream regulated gene 1 (Ndrg1) (46), and an Atf3 target gene, glutathione-specific γ-glutamylcyclotransferase 1 (Chac1) (47), were both identified as transcripts of interest (Table 2). Levels of Atf3 mRNA fell after induction of PAM expression in iPAM cells (based on RNA-seq data and qPCR analysis) (Fig. 5A). Based on RNA-seq analysis, levels of Ndrg1 mRNA were also lower after doxycycline induction of PAM expression (Fig. 5B). In contrast, levels of Chac1 mRNA were increased following induction of PAM expression in iPAM cells (Fig. 5C). qPCR analysis of both AtT-20/PAM lines vs Wt cells confirmed the decline in Atf3 and Ndrg1 transcripts and the rise in Chac1 transcripts.

In agreement with the mRNA changes, Atf3 protein levels were lower in both PAM lines than in Wt AtT-20 cells (Fig. 5D). Atf3 generally represses transcription from promoters with ATF binding sites (48). We were unable to detect Ndrg1 or Chac1 protein in AtT-20 lysates, but the reduced level of Ndrg1 mRNA observed in cells expressing high levels of PAM could contribute to the observed drop in Atf3 expression. With Atf3 acting as a repressor, levels of Chac1 mRNA would be expected to rise, as observed. Chac1 degrades glutathione, leading to its depletion and contributing to oxidative stress. PAM, which converts ascorbate into semidehydroascorbate as it generates amidated peptides, relies on reducing equivalents transferred from the cytosol to the secretory pathway lumen by cytochrome b_{561} (49), and changes in glutathione levels could affect this process.

Expression of Atf3 is regulated by stressful stimuli; its roles are generally tissue specific (50). In *Drosophila*, Atf3 is a key factor in the integration of metabolic and immune responses (51). Consistent with this observation, amino acid limitation increases ATF3 expression in HepG2 hepatoma cells (52). In a β-cell line, Atf3 is necessary for high glucose to decrease Pdx1 expression (53), and a direct interaction of Atf3 with Pdx1 contributes to β-cell dysfunction caused by endoplasmic reticulum (ER) stress (54). Eliminating cardiomyocyte Atf3 expression makes mice

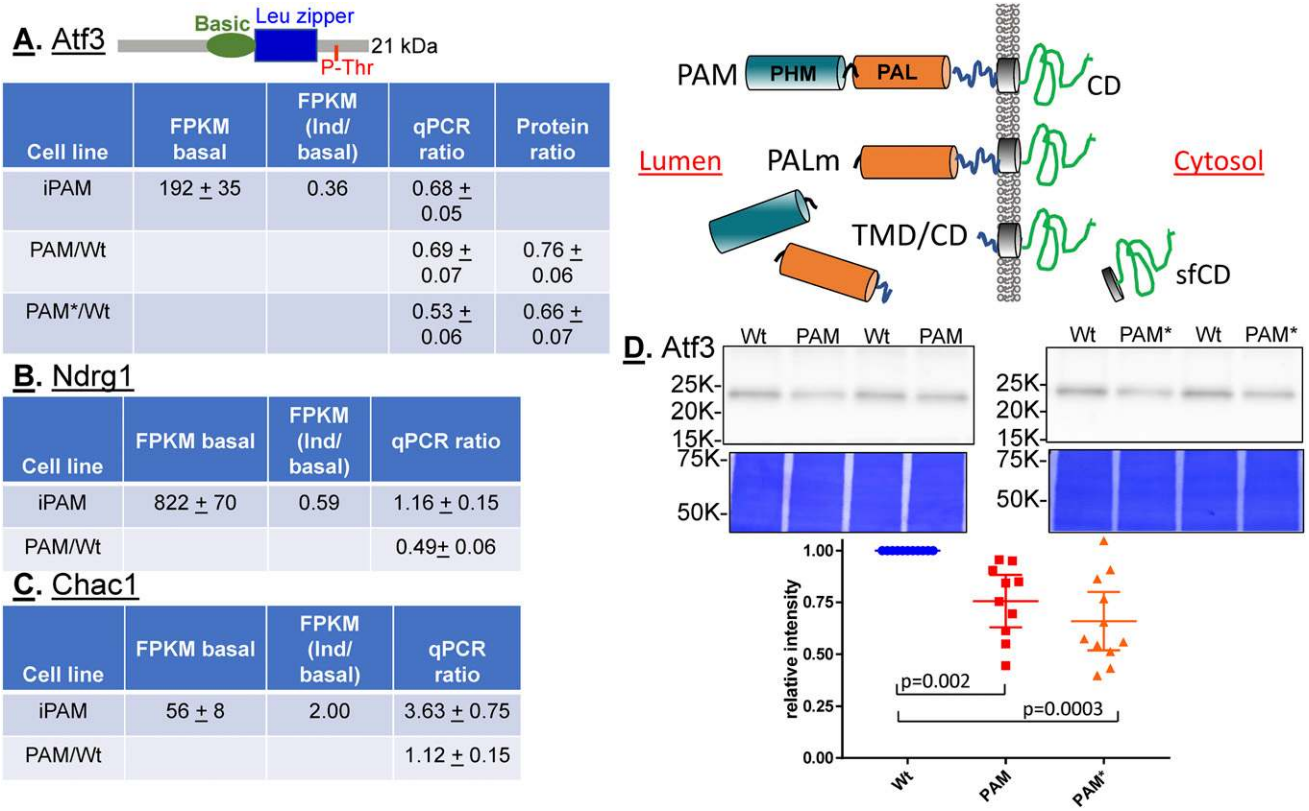

A. Atf3

Cell line	FPKM basal	FPKM (Ind/ basal)	qPCR ratio	Protein ratio
iPAM	192 ± 35	0.36	0.68 ± 0.05	
PAM/Wt			0.69 ± 0.07	0.76 ± 0.06
PAM*/Wt			0.53 ± 0.06	0.66 ± 0.07

B. Ndrg1

Cell line	FPKM basal	FPKM (Ind/ basal)	qPCR ratio
iPAM	822 ± 70	0.59	1.16 ± 0.15
PAM/Wt			0.49± 0.06

C. Chac1

Cell line	FPKM basal	FPKM (Ind/ basal)	qPCR ratio
iPAM	56 ± 8	2.00	3.63 ± 0.75
PAM/Wt			1.12 ± 0.15

Figure 5. Transcription factors. (A) Basal Atf3 FPKM data, ratio of induced/basal Atf3 FPKM values, qPCR of Atf3 transcripts in PAM and PAM* vs Wt AtT-20 cells is the average of Atf3/reference standard for each cell line (at least 10 determinations per cell line; SEM <10% of the mean); ratio of Atf3 protein levels in PAM and PAM* vs Wt AtT-20 cells from panel (D). Diagram illustrating the proteolytic processing that produces sfCD from PAM-1: the cleavage separating PHM from PAL occurs in secretory granules; cleavages separating PAL from transmembrane domain/ cytosolic domain (TMD/CD) occur in the biosynthetic and endocytic pathways, allowing γ-secretase to generate sfCD in the endocytic pathway (12). (B, C) As in panel (A), FPKM and qPCR data for Ndrg1 and Chac1. The antibodies tested failed to yield a clear signal of the expected mass. (D) SDS-lysates prepared from Wt, PAM, and PAM* AtT-20 cells (30 μg protein) were subjected to Western blot analysis; the Coomassie-stained upper part of both membranes is shown, confirming equal sample loading. Protein quantification as in Fig. 4.

kept on a high-fat diet hyperglycemic and insulin resistant (55).

Transcripts encoding secretory pathway proteins. Transcripts in this category were selected for study because secretory pathway function is clearly altered when expression of PAM is increased.

Fkbp2 (Fkbp13). Peptide bonds to proline (Xaa-Pro) are much more likely to adopt a *cis*-conformation than other peptide bonds, and 5% to 7% of the Xaa-Pro bonds in proteins do so (56). Spontaneous *cis/trans* isomerization occurs slowly (milliseconds to seconds), making this a rate-limiting step in protein folding. Binding to client proteins, peptidyl prolyl isomerases (PPIases) facilitate isomerization (57). PPIases fall into three families: FK506 binding proteins (FKBPs), immunophilins, and parvulins; secretory pathway PPIases include six FKBP family members and two immunophilin family members (58, 59).

Transcripts encoding all six secretory pathway–targeted FKBPs were detected in AtT-20 cells; Fkbp2, by far the most abundant of these, was the only transcript whose levels were regulated in response to changes in PAM expression (Fig. 6A). Fkbp2 mRNA levels rose after doxycycline induction of iPAM cells and were also higher in both AtT-20/PAM lines than in Wt cells (Fig. 6A). Fkbp2 is a small protein with a signal sequence, PPIase domain, and ER retention signal. Fkbp2 protein levels were higher in both AtT-20/PAM lines than in Wt cells (Fig. 6A).

In pancreatic islets from mice with type 2 diabetes mellitus and ER stress, levels of Fkbp2 and another ER-targeted PPIase, Fkbp11, were increased over control (60). The selective effect of increased PAM expression on Fkbp2 suggests a role for this specific FKBP in the folding of yet to be identified client proteins. The crystal structures of PHM and PAL contain no *cis*-prolyl bonds (PDB ID: 1PHM; 3FVZ).

Sec61β. Sec61, a universally conserved protein-conducting channel in the ER membrane, translocates secretory proteins and inserts proteins into the membrane (61). A small tail-anchored protein, Sec61*β*, interacts directly with the 25-kDa subunit of signal peptidase and is situated near the

A. Fkbp2 (Fkbp13)

transcript	FPKM iPAM Basal	FPKM (ind/ basal)	iPAM qPCR ratio	PAM/Wt qPCR ratio
Fkbp2 (Fkbp13)	114 ± 5	1.41	1.26	1.24
Fkbp7 (Fkbp23)	5.2 ± 0.7	0.96		
Fkbp9 (Fkbp60)	*0.03 ± 0.05*	--		
Fkbp10 (Fkbp65)	*0.2 ± 0.1*	--		
Fkbp11 (Fkbp19)	11 ± 2	1.2		
Fkbp14 (Fkbp22)	8.9 ± 2.9	0.80		
Ppib	263 ± 29	1.33 (NS)		
Ppic	*0*	--		

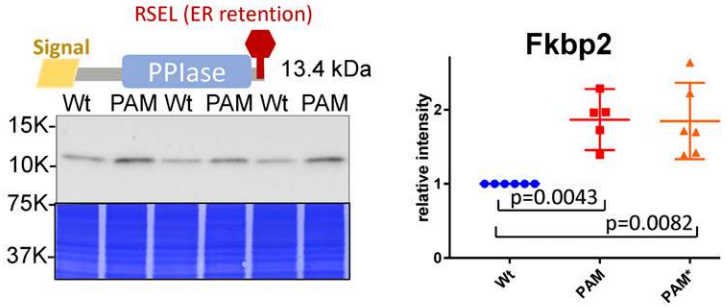

B. Sec61β

Cell line	FPKM iPAM Basal	FPKM (Ind/ basal)	qPCR ratio
iPAM	178 ± 6	1.74	1
PAM			0.65
PAM*			0.61

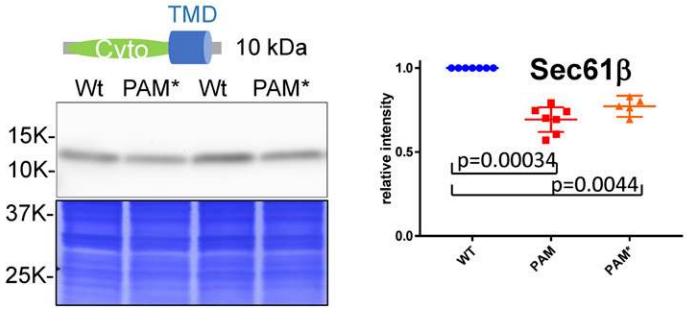

Figure 6. Secretory pathway proteins. (A) Basal FPKM data and induced/basal FPKM ratios are shown for the six FKBP and two immunophilin PPIase family members that localized to the ER. Major transcripts that did not vary significantly are on light blue background; the transcript that was regulated is in red type on a yellow background; transcripts with very low FPKM values are italicized on a gray background. Fkbp2 qPCR data are shown for iPAM and AtT-20/PAM vs Wt cells. Diagram illustrating key features of the Fkbp2 protein. Western blot analysis of Fkbp2 in Wt vs AtT-20/PAM lysates (20 μg protein); similar analyses were carried out for Wt vs AtT-20/PAM* lysates (not shown). (B) Basal FPKM data and induced/basal ratios are shown for Sec61β along with qPCR analyses of Sec61β transcripts in iPAM, Wt, PAM, and PAM* lines. Diagram illustrating key features of the Sec61β protein. Western blot analysis of Sec61β in Wt vs AtT-20/PAM* lysates; similar analyses were carried out for Wt vs AtT-20/PAM lysates (not shown). Quantification of Western blot data for both AtT-20/PAM and AtT-20/PAM* lines. NS, not significant; RSEL, Arg-Ser-Glu-Leu.

lateral opening of the translocon channel (61). Sec61β also plays an essential role in retro-translocation of misfolded proteins out of the ER for proteasomal degradation.

Our RNA-seq data indicated that levels of Sec61β mRNA were increased after exposure of iPAM cells to doxycycline. Although qPCR analysis of similar iPAM RNA samples revealed no change in Sec61β mRNA levels (Fig. 6B), the role of Sec61β in copper homeostasis (62) and the dependence of PAM on copper prompted us to analyze Sec61β mRNA levels in both AtT-20/PAM lines and Wt cells. Stable PAM expression led to a decrease in Sec61β transcripts (Fig. 6B) and Sec61β protein (Fig. 6B).

Transcripts encoding endosomal/lysosomal proteins. In cells lacking secretory granules, PAM is largely localized within the endosomal system, cycling from the trans-Golgi network to the plasma membrane and back (45). Luminal domain *O*-glycosylation of PAM and phosphorylation of its cytosolic domain determine whether PAM, internalized from the plasma membrane, enters the intraluminal vesicles of multivesicular bodies, where it is recycled or degraded (6, 63).

Cd68. Cd68, also known as macrosialin or Lamp4, is one of five members of the lysosomal/endosomal-associated membrane glycoprotein (LAMP) family; transcripts encoding Lamps 1 and 2 were more prevalent in AtT-20 cells, whereas transcripts encoding Lamps 3 and 5 were barely detectable (Fig. 7A). Cd68, a heavily glycosylated type 1 integral membrane protein, has a luminal domain with a Ser/Thr-rich mucin-like domain, a proline-rich hinge region, and a membrane proximal Lamp-like domain (Fig. 7A). Cd68 contains *N*- and *O*-glycans, which together account for over half of its mass (64).

RNA-seq identified Cd68 as one of the most down-regulated transcripts in iPAM cells following PAM induction (Table 2); qPCR analysis confirmed this conclusion for AtT-20/PAM cells vs Wt cells (Fig. 7A). Studies of Cd68 have focused on macrophages, where Western blot analysis identified cross-reactive proteins ranging in size from 87 to 115 kDa (64); the Cd68 transcript encodes a 35-kDa

peptide backbone. Western blot analysis of AtT-20 lysates revealed a complex pattern of cross-reactive material, with a major band of 75 kDa and additional bands at 38 and 48 kDa (Fig. 7A); glycosylation of Cd68 is less extensive in AtT-20 cells than in macrophages. Total Cd68 protein levels and levels of two smaller cross-reactive proteins were reduced in both AtT-20/PAM lines compared with Wt cells (Fig. 7A).

Although detected in many cells, including fibroblasts and endothelial cells, Cd68 function has only been examined in monocytes and macrophages. PAM-1 and Cd68, both type 1 integral membrane glycoproteins, cycle to and from the cell surface. Cd68 glycosylation is altered dramatically in response to zymosan internalization in macrophages, suggesting an important functional role for this posttranslational modification (65). Mutation of *O*-linked glycosylation sites in PAM-1 prevented its recycling to secretory granules and led to its rapid degradation following internalization (63). Studies using Cd68 knockout mice suggest that Cd68 regulates the movement of major histocompatibility complex II from multivesicular bodies, where major histocompatibility complex is loaded with antigen, to the cell surface (66). The fact that PAM accumulates in the intraluminal vesicles of multivesicular bodies following endocytosis identifies this as a site where these proteins could interact (45).

Autophagy-related protein 9b. Autophagy-related protein 9b (Atg9b), the only conserved transmembrane protein essential for autophagy, a degradative pathway essential for life from yeast to mammals, plays a crucial role in organizing the preautophagosomal structure (67). Vertebrates have two *ATG9* paralogues (overall identity 46%) (68). Although ATG9A is ubiquitously expressed, ATG9B expression is largely limited to placenta and pituitary. In COS7 cells, epitope-tagged Atg9a and Atg9b were similarly localized and Atg9b restored autophagy in Atg9a/9b-knockout cells.

Transcripts encoding both *Atg9* paralogues were detected at similar levels in basal iPAM AtT-20 cells (Fig. 7B). Levels of transcripts encoding Atg9b fell when expression of PAM was induced (Table 2, Fig. 5A); levels of transcripts encoding Atg9a were not affected. Except for Atg14, whose transcript levels also fell upon doxycycline induction, expression of more than a dozen other Atg transcripts identified in AtT-20 cells did not vary in response to PAM expression (Fig. 7B). A similar decline

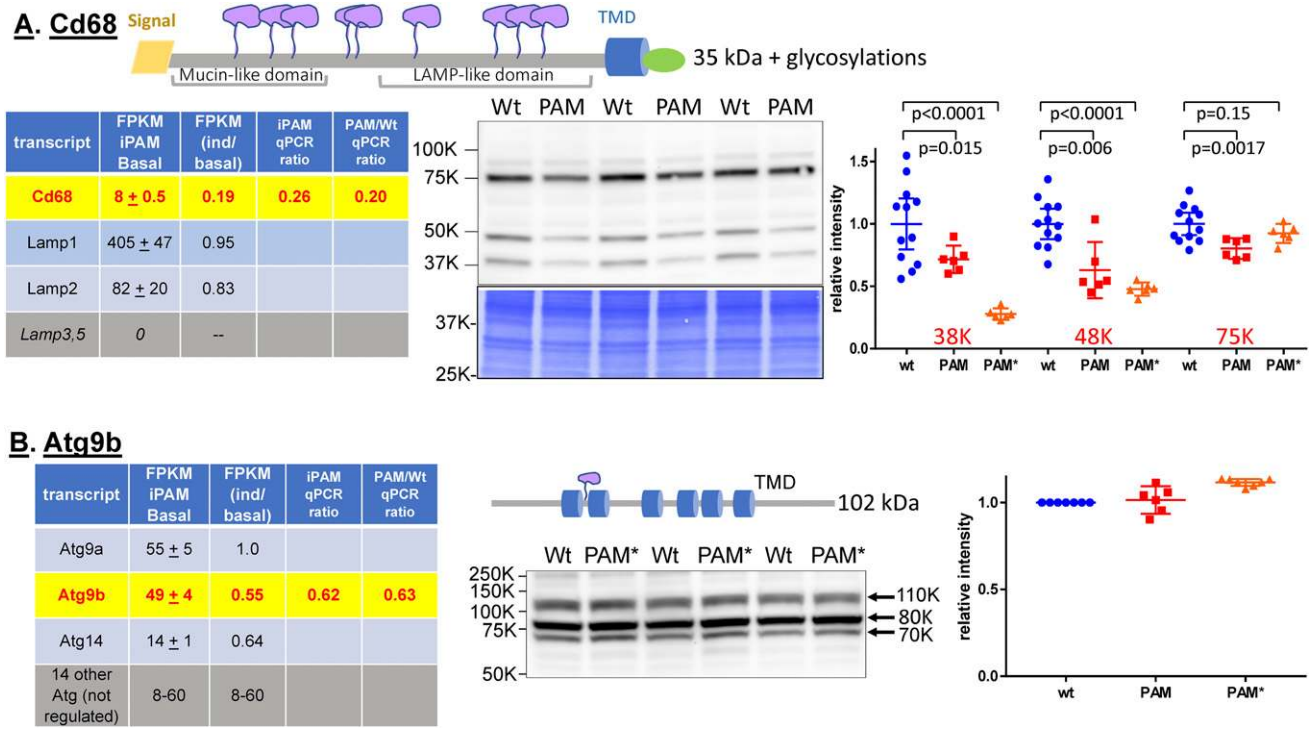

Figure 7. Endosomal/lysosomal pathway proteins. (A) Basal FPKM data and induced/basal FPKM ratios are shown for relevant Lamp family members using the color code described for Fig. 6; Cd68 qPCR ratios are shown for iPAM and AtT-20/PAM vs Wt cells. Diagram illustrating key features of the Cd68 protein. Western blot analysis of Cd68 in Wt vs PAM/AtT-20 lysates; similar analyses were carried out for Wt vs PAM*/AtT-20 lysates (not shown). Quantification of Western blots for both PAM and PAM*/AtT-20 lysates is shown. (B) Basal FPKM data and induced/basal FPKM ratios are shown for Atg family members along with qPCR analyses of Atg9b transcripts in iPAM and AtT-20/PAM vs Wt cells. Diagram illustrating key features of Atg9b. Western blot analysis of Atg9b in Wt vs PAM*/AtT-20 lysates; similar analyses were carried out for Wt vs PAM/AtT-20 lysates (not shown). Quantification of Western blots for both PAM and PAM*/AtT-20 lysates is shown.

in Atg9b transcript levels was observed in the AtT-20/PAM line vs Wt cells (Fig. 7B).

Western blot analysis using an antibody specific for a synthetic peptide unique to the C-terminal cytosolic domain of Atg9b identified cross-reactive proteins of 110, 80, and 70 kDa in AtT-20 lysates (Fig. 7B). Intact Atg9b has a predicted mass of 102 kDa, and *N*-glycosylation would increase its mass, suggesting that the 110-kDa band is intact in Atg9b; proteolytic cleavages in the *N*-terminal cytosolic domain could generate the smaller cross-reactive proteins. Cross-reactive ATG9A proteins of similar size were observed in HeLa and hEK293 cells (69). Despite the reduction in Atg9b transcript levels in cells expressing high levels of PAM, total Atg9b protein levels did not decline; similar products were detected in both AtT-20/PAM lines. An increase in Atg9b mRNA translation rate or a decrease in Atg9b protein turnover could maintain protein levels. In a recent proteomic study (60), transcripts encoding 154 islet proteins whose levels changed in response to a high-fat diet were assessed; for 54% of these proteins, changes in transcript levels and protein levels were discordant.

The amount of Atg9 expressed in cells is thought to control the frequency of autophagosome formation (67). Atg9 trafficking differs in fed vs nutrient-depleted yeast (69). In fed cells, Atg9 is localized with TGN markers in the juxtanuclear area and with endosomal markers in peripheral puncta. During starvation, Atg9 cycles between the juxtanuclear Golgi network region, peripherally situated late endosomes, and LC3-positive autophagosomes (69, 70). It is intriguing that Atg9 traverses many of the same subcellular compartments through which PAM passes during its retrieval from the cell surface.

Transcripts encoding cytosolic proteins. Several cytosolic proteins (Rho GDP/GTP exchange factors, a protein kinase, a component of the adaptor protein 1 complex t) affect PAM trafficking by interacting with its cytosolic domain (71). Interestingly, the cytosolic protein encoding transcripts identified here link PAM expression to a wide variety of metabolic pathways.

Fkbp4 (also Fkbp52; Fkbp59). Transcripts encoding cytosolic PPIases from all three families were present in the AtT-20 RNA-seq data set (Supplemental Table 1); only expression of Fkbp4, an active, multidomain cytosolic PPIase (72), was altered in response to increased PAM expression (Fig. 8A). Fkbp4 mRNA levels rose after induction of iPAM cells and were higher in AtT-20/PAM cells than in Wt cells (Table 2, Fig. 5A). Fkbp4 contains two PPIase domains followed by three tetratricopeptide repeats (TPRs), which form scaffolds that mediate protein-protein interactions (72). The first PPIase domain in Fkbp4 is an active rotamase; although not active, the second PPIase domain is essential to function (73). Consistent with the changes observed in transcript levels, Western blot analysis revealed that Fkbp4 protein levels were higher in both AtT-20/PAM lines than in Wt cells (Fig. 8A). The transcription factor Trp53 has a large number of activities relevant to this transcript data set, including the increased expression of Fkbp4 (Supplemental Fig. 2).

Glucocorticoids are major regulators of corticotrope secretion, and FKBP4 acts as a positive regulator of glucocorticoid receptor activity (73, 74). The TPR domains of FKBP4 mediate its interactions with the C-terminus of heat shock protein 90 (Hsp90). In the hormone-free state, glucocorticoid receptors form large complexes with Hsp90 and one of several cochaperone TPR proteins such as FKBP4 and FKBP5, which compete for binding. FKBP4 stabilizes steroid receptors and promotes their entry into the nucleus; the ability of FKBP4 to bind to dynein, a minus end-directed microtubule motor, plays an essential role in their nuclear trafficking (73). Through its ability to interact with Hsp90, Fkbp4 also plays a role in loading small RNA duplexes into the Ago2 RNA-induced silencing complex (75).

FKBP4 heterozygous mice have made it possible to extend *in vitro* studies to the more complex *in vivo* model (74). When adult male FKBP4$^{+/-}$ and control mice were kept on a high-fat diet, insulin levels were much higher in FKBP4$^{+/-}$ mice, which became insulin resistant and hyperglycemic. Strikingly, the livers of the FKBP4$^{+/-}$ mice appeared to be glucocorticoid resistant: lipid content high, lipogenic gene expression elevated, and gluconeogenic gene expression reduced, despite elevated serum corticosterone levels. FKBP4 expression is normally high in the liver but almost undetectable in skeletal muscle and adipose tissue, contributing to what looks like a liver-specific loss of glucocorticoid receptor activity.

The Fkbp family of proteins bind FK-506 and cyclosporin A, and ACTH secretion from AtT-20 cells has been reported to be stimulated by these drugs (76). Our data did not show significant stimulation or inhibition of ACTH secretion by these drugs at the concentrations reported in the literature (Supplemental Fig. 3).

Thioredoxin-interacting protein). Thioredoxin-interacting protein (Txnip), a member of the α-arrestin family, was first discovered as the most glucose-induced gene in human islets and was later identified through its ability to bind to and inhibit thioredoxin (77, 78). The arrestin-fold is shared by β-arrestins, regulators of G protein–coupled receptor signaling and trafficking, and by α-arrestins, a more ancient and less well-studied family. The C-termini of α-arrestins bind to E3 ubiquitin ligases, an interaction that affects their turnover. A single

A. Non-ER-targeted Fkbps

transcript	FPKM iPAM Basal	FPKM (ind/ basal)	iPAM qPCR ratio	PAM/Wt qPCR ratio
Fkbp1a (Fkbp12)	414 ± 113	1.06		
Fkbp1b (Fkbp12.6)	*2.0 ± 0.8*	*0.6*		
Fkbp3 (Fkbp25)	350 ± 24	1.02		
Fkbp4 (Fkbp52)	**134 ± 5**	**1.57**	**1.60**	**1.61**
Fkbp5 (Fkbp51)	62 ± 2	0.95		
Fkbp6 (Fkbp36)	*0*	--		
Fkbp8 (Fkbp38)	196 ± 29	1.00		
Fkbp15 (Fkbp133)	21 ± 6	1.1		

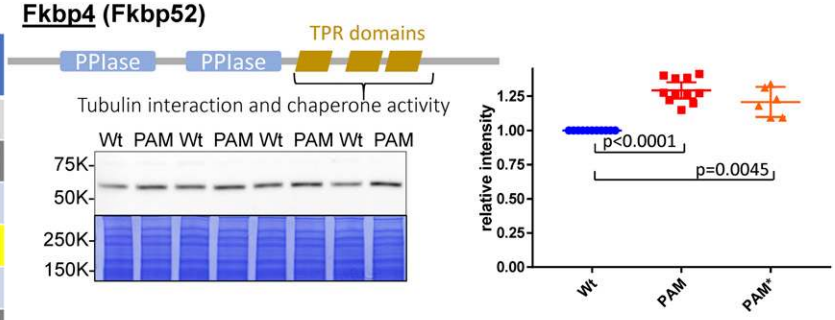

B. Txnip

Cell line	FPKM basal	FPKM (Ind/ basal)	qPCR ratio
iPAM	638 ± 61	0.39	0.58
PAM/Wt			0.40
PAM*/Wt			0.36

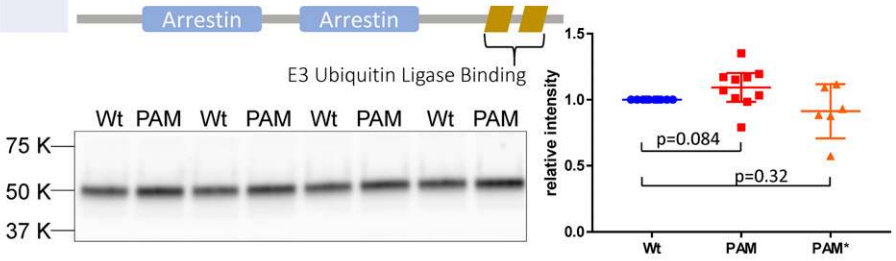

Figure 8. Cytosolic proteins. (A) Basal FPKM data and induced/basal FPKM ratios are shown for relevant non-ER–targeted FKBP family members using the color code described for Fig. 6; Fkbp4 qPCR ratios are shown for iPAM and AtT-20/PAM vs Wt cells. Diagram illustrating key features of the Fkbp4 protein. Western blot analysis of Fkbp4 in Wt vs AtT-20/PAM lysates; similar analyses were carried out for Wt vs AtT-20/PAM* lysates (not shown). Quantification of Western blots for both PAM and PAM*/AtT-20 lysates is shown. (B) For Txnip in iPAM cells, basal FPKM data and the induced/basal FPKM ratio are shown; qPCR ratios for Txnip in both PAM-1 AtT-20 lines vs Wt cells are shown. Western blot analysis of Txnip in AtT-20/PAM vs Wt lysates is shown; similar analyses were carried out for AtT-20/PAM* vs Wt lysates (not shown). Quantification of Western blots for both PAM and PAM*/AtT-20 lysates is shown.

cysteine-to-serine mutation in Txnip eliminates its ability to bind and inhibit thioredoxin but inhibits only a subset of its other functions (79).

Expression of transcripts encoding Txnip declined after induction of iPAM cells and was lower in both AtT-20/PAM lines than in Wt cells (Fig. 8B). Despite these changes in transcript levels, Western blot analysis revealed no change in Txnip protein in either AtT-20/PAM line in comparison with Wt cells (Fig. 8B). Based on studies in other systems, levels of Txnip protein reflect changes in transcription, mRNA, and protein stability; for example, thioredoxin binding increases Txnip half-life (77, 78).

Txnip is widely expressed and responds to nutritional status and other signals in a tissue-specific manner (80). A key player in β-cell biology, Txnip acts as a negative feedback regulator of glucose uptake. Blood glucose and insulin levels are low in Txnip null mice; on a high-fat diet, these mice gain more adipose tissue mass than controls, and the ability of insulin to increase glucose uptake into skeletal muscle and adipocytes is enhanced (81, 82). The ability of insulin to promote Txnip/thioredoxin dissociation increases Txnip turnover and promotes adipogenesis.

The Txnip/thioredoxin system links pathways that control antioxidant defense, cell survival, and energy metabolism (78). Txnip, which interacts with von Hippel-Lindau protein and has a putative hypoxia-responsive element in its promoter, plays a key role in tuning overall metabolism to the amount of oxygen available. The fact that Txnip protein levels in AtT-20 cells were unchanged in response to altered levels of PAM, despite a ~2.5-fold drop in Txnip mRNA, suggests a decrease in its turnover. The inputs governing the set point for Txnip expression in different cells are not understood.

Pathway and network analysis: Limma, DESeq2, and CuffSig

We turned to pathway analysis to explore further our hypothesis that the identification of genes whose expression responded to changes in PAM expression would reveal fundamental pathways not currently recognized as major contributors to the control of basal or stimulated peptide secretion. Pathway analysis using IPA was performed using a list of 442 transcripts derived by combining transcripts identified by Limma or DESeq (281 transcripts) and a variance-limited CuffSig group (320 transcripts, 159 of which were already in the Limma plus DESeq set) (see Materials and Methods). We looked first at the most regulated canonical pathways (Supplemental Table 2). Increased PAM expression was associated with inhibition of nine canonical signaling pathways; none were activated. Almost all of these involved cell-to-cell

signaling, perhaps reflecting commonalities in the molecular bases of signaling by pituitary cells, neurons, and many other cells and tissues. Autocrine growth factors, which are often amidated, could play a role in several of the canonical pathways identified (glioblastoma multiforme, cholecystokinin/gastrin, colorectal cancer). An association of PAM with IL-8 signaling or integrin-mediated signaling has not yet been explored.

Several regulatory interrelationships were suggested by the IPA program (Fig. 9, Supplemental Table 2 and Supplemental Fig. 2). For each of the examples shown in Fig. 9, the upstream regulator at the center of the diagram can be tied directly or indirectly to several downstream target genes whose levels of expression were altered in a manner consistent with altered function of the upstream regulator. None of the five upstream regulator molecules depicted showed a significant change in RNA expression in response to doxycycline induction of PAM expression, but each is expressed at a substantial level in AtT-20 cells (fold-change and FPKM values shown in Fig. 9), and each is known to be activated or inhibited by posttranslational modifications such as phosphorylation. cAMP-responsive element binding protein 1 (Creb1), a leucine zipper DNA binding protein, is the target of several protein kinases. Each of the Creb1 targets identified showed decreased transcript levels in the induced iPAM cells, which could occur as a direct effect of diminished Creb1 activation. Inhibition of Kdm5a (lysine demethylase 5A), a member of the Jumonji, AT-rich interactive domain histone demethylase family, which often functions as a negative regulator of transcription, could lead to the observed increase in expression of each of the target genes shown. Like the HIF prolyl hydroxylases, Kdm5a is a 2-oxoglutarate dependent dioxygenase; a role for PAM in regulating this pathway is consistent with the suggestion that this oxygen-dependent enzyme also plays a role in the response of cells to oxygen availability.

The other three interactions shown only indirectly connect each upstream regulator to the targets shown (Fig. 9, lower, dashed lines). Toll-like receptor 3 (Tlr3) is a nucleotide-sensing Toll-like receptor with a C2 Ig-like domain and leucine-rich repeats. Expressed in the placenta and pancreas, Tlr3 activates NF-κB, cytokine secretion, and the inflammatory response. The PAM-mediated decrease in Atf3 expression could reflect decreased Creb1 activity or lowered Tlr3 activity (Fig. 9). Mapk3/1 (mitogen-activated protein kinases; Erk1/2, extracellular signal-regulated kinases) is activated by phosphorylation, translocating to the nucleus. Expression of the four Mapk/Erk targets shown decreased in cells expressing high levels of PAM. Myeloid differentiation primary response 88 (Myd88) has an *N*-terminal death domain preceding its C-terminal

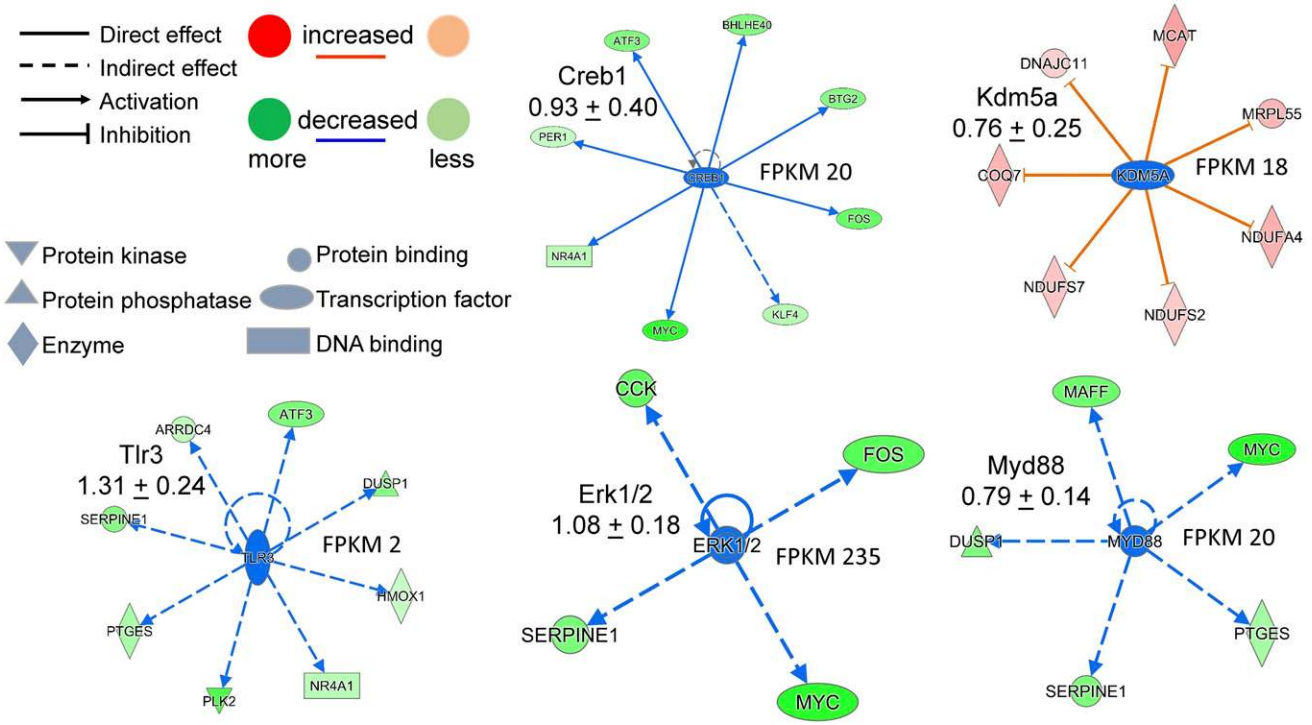

Figure 9. Pathway and network analysis of differentially expressed genes. IPA (Qiagen) was used with a composite of the Limma, DESeq2, and Cuffsig differentially regulated genes. IPA accepts the transcript list with the log2(fold change) from the RNA-seq data and provides an extensively annotated output, including pathways and networks of interacting molecules. Symbols indicate direct/indirect effects; activation/inactivation. Color indicates direction/magnitude of change. Symbol shape identifies major function of each gene.

Toll–IL-1 receptor domain and plays a central role in innate and adaptive immunity. Expression of each of the Myd88 target transcripts shown decreased when PAM expression was high. Additional potential upstream regulators are shown in Supplemental Fig. 2. A set of genes involved in mitochondrial energy generation and the proteasome was identified as the most downregulated set, with rapamycin-insensitive companion of mTOR as the upstream regulator.

Discussion

The original hypothesis of this study was that a systems-level identification of genes whose expression responded to changes in PAM expression would reveal fundamental pathways not currently recognized as major contributors to the control of peptide secretion. Our data provide support for this hypothesis and identify specific ways in which this hypothesis can be further explored. Expression of PAM diminished Gapdh expression, with potential effects on energy utilization. The increased expression of Fkbp2, a luminal prolyl isomerase, whose expression is known to increase in type II diabetes and during ER stress, suggests the existence of client proteins whose expression is induced by PAM. Changes observed in a pathway involving Ndrg1, Atf3, and Chac1 could alter glutathione levels, reflecting the fact that the PAM reaction produces dehydroascorbate. Changes observed in the expression of proteins involved in multivesicular body function (Cd68) and autophagy (Atg9b) are consistent with the suggestion that PAM has roles in the endocytic and biosynthetic pathways. Especially interesting was the observed increase in the expression of Fkbp4, a mediator of glucocorticoid receptor function with a clear role in metabolic integration. Demonstrated reductions in Atf3 expression in response to increased expression of PAM could link PAM to multiple pathways important to metabolic regulation, immune function, and amino acid deprivation. The fact that many of the genes whose expression was affected by increased PAM expression are known to respond to oxygen availability provides further support for our hypothesis. PAM expression, which is tightly controlled during development (83, 84) and responds in a tissue-specific manner to endocrine and environmental inputs (85, 86), may be integrated into the many pathways needed to coordinate metabolic changes.

Acknowledgments

We thank Michael O. Duff, Alissa Resch, and Sara Olson Peterson for invaluable help performing the library construction, sequencing, and Cuffdiff analysis, as well as Taylor LaRese and Kathryn Powers for innumerable SDS gels and help with tissue culture.

Financial Support: This work was supported by National Institutes of Health Grants DA-035474 and DK-032948 (to R.E.M. and B.A.E.).

Author Contributions: R.E.M. and B.A.E. conceived, designed, and performed the experiments; R.E.M., B.A.E., C.B.-H., and B.A.R. analyzed the data; and R.E.M., B.A.E., and C.B.-H. drafted the article and prepared the digital images.

Correspondence: Richard E. Mains, PhD, University of Connecticut Health Center, 263 Farmington Avenue, Farmington, Connecticut 06030. E-mail: mains@uchc.edu.

Disclosure Summary: The authors have nothing to disclose.

References

1. Brandwein M, Bentwich Z, Steinberg D. Endogenous antimicrobial peptide expression in response to bacterial epidermal colonization. *Front Immunol*. 2017;**8**:1637.
2. Broderick NA. Friend, foe or food? Recognition and the role of antimicrobial peptides in gut immunity and Drosophila-microbe interactions. *Philos Trans R Soc Lond B Biol Sci*. 2016;**371**(1695): 20150295.
3. Pisoschi AM, Pop A, Georgescu C, Turcuş V, Olah NK, Mathe E. An overview of natural antimicrobials role in food. *Eur J Med Chem*. 2018;**143**:922–935.
4. Shabir U, Ali S, Magray AR, Ganai BA, Firdous P, Hassan T, Nazir R. Fish antimicrobial peptides (AMP's) as essential and promising molecular therapeutic agents: a review. *Microb Pathog*. 2018;**114**: 50–56.
5. Kumar D, Blaby-Haas CE, Merchant SS, Mains RE, King SM, Eipper BA. Early eukaryotic origins for cilia-associated bioactive peptide-amidating activity. *J Cell Sci*. 2016;**129**(5):943–956.
6. Kumar D, Mains RE, Eipper BA. 60 Years of POMC: from POMC and α-MSH to PAM, molecular oxygen, copper, and vitamin C. *J Mol Endocrinol*. 2015;**56**(4):T63–T76.
7. Kumar D, Strenkert D, Patel-King RS, Leonard MT, Merchant SS, Mains RE, King SM, Eipper BA. A bioactive peptide amidating enzyme is required for ciliogenesis. *eLife*. 2017;**6**:e25728.
8. Dotman CH, van Herp F, Martens GJM, Jenks BG, Roubos EW. Dynamics of proopiomelanocortin and prohormone convertase 2 gene expression in Xenopus melanotrope cells during long-term background adaptation. *J Endocrinol*. 1998;**159**:281–286.
9. Attenborough RM, Hayward DC, Kitahara MV, Miller DJ, Ball EEA. A "neural" enzyme in nonbilaterian animals and algae: preneural origins for peptidylglycine α-amidating monooxygenase. *Mol Biol Evol*. 2012;**29**(10):3095–3109.
10. Gould SB, Garg SG, Martin WF. Bacterial vesicle secretion and the evolutionary origin of the eukaryotic endomembrane system. *Trends Microbiol*. 2016;**24**(7):525–534.
11. Rout MP, Field MC. The evolution of organellar coat complexes and organization of the eukaryotic cell. *Annu Rev Biochem*. 2017; **86**(1):637–657.
12. Rajagopal C, Mains RE, Eipper BA. Signaling from the secretory granule to the nucleus. *Crit Rev Biochem Mol Biol*. 2012;**47**(4): 391–406.
13. Ciccotosto GD, Schiller MR, Eipper BA, Mains RE. Induction of integral membrane PAM expression in AtT-20 cells alters the storage and trafficking of POMC and PC1. *J Cell Biol*. 1999; **144**(3):459–471.
14. Francone VP, Ifrim MF, Rajagopal C, Leddy CJ, Wang Y, Carson JH, Mains RE, Eipper BA. Signaling from the secretory granule to the nucleus: Uhmk1 and PAM. *Mol Endocrinol*. 2010;**24**: 1543–1558.
15. Simpson PD, Eipper BA, Katz MJ, Gandara L, Wappner P, Fischer R, Hodson EJ, Ratcliffe PJ, Masson N. Striking oxygen sensitivity

of the peptidylglycine α-amidating monooxygenase (PAM) in neuroendocrine cells. *J Biol Chem*. 2015;**290**(41):24891–24901.
16. Oldham CD, Li C, Feng J, Scott RO, Wang WZ, Moore AB, Girard PR, Huang J, Caldwell RB, Caldwell RW, May SW. Amidative peptide processing and vascular function. *Am J Physiol*. 1997; **273**(6):C1908–C1914.
17. Saldise L, Martínez A, Montuenga LM, Treston A, Springall DR, Polak JM, Vázquez JJ. Distribution of peptidyl-glycine alpha-amidating mono-oxygenase (PAM) enzymes in normal human lung and in lung epithelial tumors. *J Histochem Cytochem*. 1996;**44**(1):3–12.
18. Mains RE, Eipper BA. Peptides. In: Brady ST, Siegel GJ, Albers RW, Price DL, eds. *Basic Neurochemistry Principles of Molecular, Cellular and Medical Neurobiology*. 8th ed. Cambridge, MA: Elsevier Academic Press; 2012:390–406.
19. Schiller MR, Mains RE, Eipper BA. A neuroendocrine-specific protein localized to the endoplasmic reticulum by distal degradation. *J Biol Chem*. 1995;**270**(44):26129–26138.
20. Milgram SL, Johnson RC, Mains RE. Expression of individual forms of peptidylglycine α-amidating monooxygenase in AtT-20 cells: endoproteolytic processing and routing to secretory granules. *J Cell Biol*. 1992;**117**(4):717–728.
21. Tausk FA, Milgram SL, Mains RE, Eipper BA. Expression of a peptide processing enzyme in cultured cells: truncation mutants reveal a routing domain. *Mol Endocrinol*. 1992;**6**(12):2185–2196.
22. May V, Eipper BA. Long term culture of primary rat pituitary adrenocorticotropin/endorphin-producing cells in serum-free medium. *Endocrinology*. 1986;**118**(4):1284–1295.
23. Mains RE, Eipper BA. Coordinate, equimolar secretion of smaller peptide products derived from pro-ACTH/endorphin by mouse pituitary tumor cells. *J Cell Biol*. 1981;**89**(1):21–28.
24. Eipper-Mains JE, Kiraly DD, Duff MO, Horowitz MJ, McManus CJ, Eipper BA, Graveley BR, Mains RE. Effects of cocaine and withdrawal on the mouse nucleus accumbens transcriptome. *Genes Brain Behav*. 2012;**12**(1):21–33.
25. Conesa A, Madrigal P, Tarazona S, Gomez-Cabrero D, Cervera A, McPherson A, Szcześniak MW, Gaffney DJ, Elo LL, Zhang X, Mortazavi A. A survey of best practices for RNA-seq data analysis. *Genome Biol*. 2016;**17**(1):13.
26. Łabaj PP, Kreil DP. Sensitivity, specificity, and reproducibility of RNA-Seq differential expression calls. *Biol Direct*. 2016;**11**(1):66.
27. Wu Z, Wu H. Experimental design and power calculation for RNA-Seq experiments. *Methods Mol Biol*. 2016;**1418**:379–390.
28. Soneson C, Delorenzi M. A comparison of methods for differential expression analysis of RNA-Seq data. *BMC Bioinformatics*. 2013; **14**(1):91.
29. Seyednasrollah F, Laiho A, Elo LL. Comparison of software packages for detecting differential expression in RNA-Seq studies. *Brief Bioinform*. 2013;**16**(1):59–70.
30. Rapaport F, Khanin R, Liang Y, Pirun M, Krek A, Zumbo P, Mason CE, Socci ND, Betel D. Comprehensive evaluation of differential gene expression analysis methods for RNA-Seq data. *Genome Biol*. 2013;**14**(9):R95.
31. Anders S, Huber W. Differential expression analysis for sequence count data. *Genome Biol*. 2010;**11**(10):R106.
32. Bullard JH, Purdom E, Hansen KD, Dudoit S. Evaluation of statistical methods for normalization and differential expression in mRNA-Seq experiments. *BMC Bioinformatics*. 2010;**11**(1):94.
33. El Meskini R, Galano GJ, Marx R, Mains RE, Eipper BA. Targeting of membrane proteins to the regulated secretory pathway in anterior pituitary endocrine cells. *J Biol Chem*. 2000;**276**(5): 3384–3393.
34. Dickerson IM, Mains RE. Cell-type specific posttranslational processing of peptides by different pituitary cell lines. *Endocrinology*. 1990;**127**(1):133–140.
35. Yun H-Y, Eipper BA. Addition of an endoplasmic reticulum retention/retrieval signal does not block maturation of enzymatically active peptidylglycine α-amidating monooxygenase. *J Biol Chem*. 1995;**270**:15412–15416.
36. Eipper BA, Mains RE. Existence of a common precursor to ACTH and endorphin in the anterior and intermediate lobes of the rat pituitary. *J Supramol Struct*. 1978;**8**(3):247–262.
37. Noel G, Keutmann HT, Mains RE. Investigation of the structural requirements for peptide precursor processing in AtT-20 cells using site-directed mutagenesis of proadrenocorticotropin/endorphin. *Mol Endocrinol*. 1991;**5**(3):404–413.
38. Douglas WW, Poisner AM. On the relation between ATP splitting and secretion in the adrenal chromaffin cell: extrusion of ATP (unhydrolysed) during release of catecholamines. *J Physiol*. 1966; **183**(1):249–256.
39. Surprenant A. Correlation between electrical activity and ACTH/ β-endorphin secretion in mouse pituitary tumor cells. *J Cell Biol*. 1982;**95**(2):559–566.
40. Klenke S, Renckhoff K, Engler A, Peters J, Frey UH. Easy-to-use strategy for reference gene selection in quantitative real-time PCR experiments. *Naunyn Schmiedebergs Arch Pharmacol*. 2016; **389**(12):1353–1366.
41. Lima L, Gaiteiro C, Peixoto A, Soares J, Neves M, Santos LL, Ferreira JA. Reference genes for addressing gene expression of bladder cancer cell models under hypoxia: a step towards transcriptomic studies. *PLoS One*. 2016;**11**(11):e0166120.
42. Zheng L, Roeder RG, Luo Y. S phase activation of the histone H2B promoter by OCA-S, a coactivator complex that contains GAPDH as a key component. *Cell*. 2003;**114**(2):255–266.
43. Webster KA. Evolution of the coordinate regulation of glycolytic enzyme genes by hypoxia. *J Exp Biol*. 2003;**206**(17): 2911–2922.
44. Del Rey MJ, Valín Á, Usategui A, García-Herrero CM, Sánchez-Aragó M, Cuezva JM, Galindo M, Bravo B, Cañete JD, Blanco FJ, Criado G, Pablos JL. Hif-1α knockdown reduces glycolytic metabolism and induces cell death of human synovial fibroblasts under normoxic conditions. *Sci Rep*. 2017;**7**(1):3644.
45. Bäck N, Kanerva K, Kurutihalli V, Yanik A, Ikonen E, Mains RE, Eipper BA. The endocytic pathways of a secretory granule membrane protein in HEK293 cells: PAM and EGF traverse a dynamic multivesicular body network together. *Eur J Cell Biol*. 2017;**96**(5): 407–417.
46. Liu W, Iizumi-Gairani M, Okuda H, Kobayashi A, Watabe M, Pai SK, Pandey PR, Xing F, Fukuda K, Modur V, Hirota S, Suzuki K, Chiba T, Endo M, Sugai T, Watabe K. KAI1 gene is engaged in NDRG1 gene-mediated metastasis suppression through the ATF3-NFkappaB complex in human prostate cancer. *J Biol Chem*. 2011; **286**(21):18949–18959.
47. Crawford RR, Prescott ET, Sylvester CF, Higdon AN, Shan J, Kilberg MS, Mungrue IN. Human CHAC1 protein degrades glutathione, and mRNA induction is regulated by the transcription factors ATF4 and ATF3 and a bipartite ATF/CRE regulatory element. *J Biol Chem*. 2015;**290**(25):15878–15891.
48. Chen BP, Liang G, Whelan J, Hai T. ATF3 and ATF3 delta zip: transcriptional repression versus activation by alternatively spliced isoforms. *J Biol Chem*. 1994;**269**(22):15819–15826.
49. Wimalasena K, Wimalasena DS. The reduction of membrane-bound dopamine beta-monooxygenase in resealed chromaffin granule ghosts: is intragranular ascorbic acid a mediator for extragranular reducing equivalents? *J Biol Chem*. 1995;**270**(46): 27516–27524.
50. Hunt D, Raivich G, Anderson PN. Activating transcription factor 3 and the nervous system. *Front Mol Neurosci*. 2012;**5**:7.
51. Rynes J, Donohoe CD, Frommolt P, Brodesser S, Jindra M, Uhlirova M. Activating transcription factor 3 regulates immune and metabolic homeostasis. *Mol Cell Biol*. 2012;**32**(19): 3949–3962.
52. Pan YX, Chen H, Thiaville MM, Kilberg MS. Activation of the ATF3 gene through a co-ordinated amino acid-sensing response programme that controls transcriptional regulation of responsive genes following amino acid limitation. *Biochem J*. 2007;**401**(1): 299–307.

53. Jang MK, Park HJ, Jung MH. ATF3 represses PDX-1 expression in pancreatic β-cells. *Biochem Biophys Res Commun*. 2011;**412**(2): 385–390.
54. Kim WH, Jang MK, Kim CH, Shin HK, Jung MH. ATF3 inhibits PDX-1-stimulated transactivation. *Biochem Biophys Res Commun*. 2011;**414**(4):681–687.
55. Kalfon R, Koren L, Aviram S, Schwartz O, Hai T, Aronheim A. ATF3 expression in cardiomyocytes preserves homeostasis in the heart and controls peripheral glucose tolerance. *Cardiovasc Res*. 2016;**113**(2):134–146.
56. Schmidpeter PA, Koch JR, Schmid FX. Control of protein function by prolyl isomerization. *Biochim Biophys Acta*. 2015;**1850**: 1973–1982.
57. Dunyak BM, Gestwicki JE. Peptidyl-proline isomerases (PPIases): targets for natural products and natural product-inspired compounds. *J Med Chem*. 2016;**59**(21):9622–9644.
58. Ishikawa Y, Boudko S, Bächinger HP. Ziploc-ing the structure: triple helix formation is coordinated by rough endoplasmic reticulum resident PPIases. *Biochim Biophys Acta*. 2015;**1850**:1983–1993.
59. Thapar R. Roles of prolyl isomerases in RNA-mediated gene expression. *Biomolecules*. 2015;**5**(2):974–999.
60. Lu H, Yang Y, Allister EM, Wijesekara N, Wheeler MB. The identification of potential factors associated with the development of type 2 diabetes: a quantitative proteomics approach. *Mol Cell Proteomics*. 2008;**7**(8):1434–1451.
61. Pfeffer S, Burbaum L, Unverdorben P, Pech M, Chen Y, Zimmermann R, Beckmann R, Förster F. Structure of the native Sec61 protein-conducting channel. *Nat Commun*. 2015;**6**(1):8403.
62. Abada PB, Larson CA, Manorek G, Adams P, Howell SB. Sec61β controls sensitivity to platinum-containing chemotherapeutic agents through modulation of the copper-transporting ATPase ATP7A. *Mol Pharmacol*. 2012;**82**(3):510–520.
63. Vishwanatha KS, Bäck N, Lam TT, Mains RE, Eipper BA. O-Glycosylation of a secretory granule membrane enzyme is essential for its endocytic trafficking. *J Biol Chem*. 2016;**291**(18): 9835–9850.
64. Holness CL, da Silva RP, Fawcett J, Gordon S, Simmons DL. Macrosialin, a mouse macrophage-restricted glycoprotein, is a member of the lamp/lgp family. *J Biol Chem*. 1993;**268**(13): 9661–9666.
65. da Silva RP, Gordon S. Phagocytosis stimulates alternative glycosylation of macrosialin (mouse CD68), a macrophage-specific endosomal protein. *Biochem J*. 1999;**338**(3):687–694.
66. Song L, Lee C, Schindler C. Deletion of the murine scavenger receptor CD68. *J Lipid Res*. 2011;**52**(8):1542–1550.
67. Hurley JH, Young LN. Mechanisms of autophagy initiation. *Annu Rev Biochem*. 2017;**86**(1):225–244.
68. Yamada T, Carson AR, Caniggia I, Umebayashi K, Yoshimori T, Nakabayashi K, Scherer SW. Endothelial nitric-oxide synthase antisense (NOS3AS) gene encodes an autophagy-related protein (APG9-like2) highly expressed in trophoblast. *J Biol Chem*. 2005; **280**(18):18283–18290.
69. Webber JL, Tooze SA. Coordinated regulation of autophagy by p38alpha MAPK through mAtg9 and p38IP. *EMBO J*. 2009;**29**(1): 27–40.
70. Takahashi Y, Meyerkord CL, Hori T, Runkle K, Fox TE, Kester M, Loughran TP, Wang HG. Bif-1 regulates Atg9 trafficking by mediating the fission of Golgi membranes during autophagy. *Autophagy*. 2011;**7**(1):61–73.
71. Miller MB, Yan Y, Eipper BA, Mains RE. Neuronal Rho GEFs in synaptic physiology and behavior. *Neuroscientist*. 2013;**19**(3): 255–273.
72. Schiene-Fischer C. Multidomain peptidyl prolyl cis/trans isomerases. *Biochim Biophys Acta*. 2015;**1850**:2005–2016.
73. Tong M, Jiang Y. FK506-binding proteins and their diverse functions. *Curr Mol Pharmacol*. 2015;**9**(1):48–65.
74. Warrier M, Hinds TD Jr, Ledford KJ, Cash HA, Patel PR, Bowman TA, Stechschulte LA, Yong W, Shou W, Najjar SM, Sanchez ER. Susceptibility to diet-induced hepatic steatosis and glucocorticoid resistance in FK506-binding protein 52-deficient mice. *Endocrinology*. 2010;**151**(7):3225–3236.
75. Martinez NJ, Chang HM, Borrajo JR, Gregory RI. The co-chaperones Fkbp4/5 control Argonaute2 expression and facilitate RISC assembly. *RNA*. 2013;**19**(11):1583–1593.
76. Sheppard KE. Cyclosporin A and FK506 are potent activators of proopiomelanocortin-derived peptide secretion without affecting corticotrope glucocorticoid receptor function. *J Neuroendocrinol*. 1995;**7**(11):833–840.
77. Shalev A. Minireview: thioredoxin-interacting protein: regulation and function in the pancreatic β-cell. *Mol Endocrinol*. 2014;**28**(8): 1211–1220.
78. Yoshioka J, Lee RT. Thioredoxin-interacting protein and myocardial mitochondrial function in ischemia-reperfusion injury. *Trends Cardiovasc Med*. 2014;**24**(2):75–80.
79. Chutkow WA, Lee RT. Thioredoxin regulates adipogenesis through thioredoxin-interacting protein (Txnip) protein stability. *J Biol Chem*. 2011;**286**(33):29139–29145.
80. Yoshihara E, Masaki S, Matsuo Y, Chen Z, Tian H, Yodoi J. Thioredoxin/Txnip: redoxisome, as a redox switch for the pathogenesis of diseases. *Front Immunol*. 2014;**4**:514.
81. Chutkow WA, Birkenfeld AL, Brown JD, Lee HY, Frederick DW, Yoshioka J, Patwari P, Kursawe R, Cushman SW, Plutzky J, Shulman GI, Samuel VT, Lee RT. Deletion of the alpha-arrestin protein Txnip in mice promotes adiposity and adipogenesis while preserving insulin sensitivity. *Diabetes*. 2010;**59**(6):1424–1434.
82. Patwari P, Lee RT. An expanded family of arrestins regulate metabolism. *Trends Endocrinol Metab*. 2012;**23**(5):216–222.
83. Ouafik L, May V, Keutmann HT, Eipper BA. Developmental regulation of peptidylglycine alpha-amidating monooxygenase (PAM) in rat heart atrium and ventricle. Tissue-specific changes in distribution of PAM activity, mRNA levels, and protein forms. *J Biol Chem*. 1989;**264**(10):5839–5845.
84. Park D, Shafer OT, Shepherd SP, Suh H, Trigg JS, Taghert PH. The *Drosophila* BHLH protein *DIMMED* directly activates *PHM*, a gene encoding a neuropeptide amidating enzyme. *J Biol Chem*. 2007;**28**(1):410–421.
85. El Meskini R, Boudouresque F, Ouafik L. Estrogen regulation of peptidylglycine α-amidating monooxygenase messenger ribonucleic acid levels by a nuclear posttranscriptional event. *Endocrinology*. 1997;**138**(12):5256–5265.
86. Ouafik L, May V, Saffen DW, Eipper BA. Thyroid hormone regulation of peptidylglycine alpha-amidating monooxygenase expression in anterior pituitary gland. *Mol Endocrinol*. 1990; **4**(10):1497–1505.